UNIVERSITY OF TROMSØ UIT

FACULTY OF SCIENCE AND TECHNOLOGY
DEPARTMENT OF PHYSICS AND TECHNOLOGY

Influence of Meteoric Aerosol Particles on the Charge Balance in the Upper Mesosphere During ECOMA 2010

Åse Svendsen

FYS-3931

Master's thesis in Space Physics

December 15, 2011

Supervised by:
Ulf-Peter Hoppe
and
Tom Arild Blix

Influence of Meteoric Aerosol Particles on the Charge Balance in the Upper Mesosphere During ECOMA 2010

Abstract
This work is focused on the three sounding rocket launches during the ECOMA Geminids campaign in December 2010: One before the Geminids meteor shower, one at its peak and one some days after the peak. In this work, the main emphasis is on analyzing the results from electron and ion probes on the rockets, obtaining electron and ion density profiles, and comparing them with the measurements of meteoric smoke particles. Aerosol particles originating from meteors may be the condensation nuclei for ice particles that form phenomena such as NLC ad PMSE. This work concludes that there area strong indications of the existence of negatively charged smoke particles in the height region between 80-95km. It describes how these parameters were measured, and how to get from raw data to the end results.

Acknowledgments

I'd like to start by thanking my main supervisor Ulf-Peter Hoppe for his guidance, patience, and help through the work with this thesis. His explanations and corrections were of great value to me.

I also want to thank my second supervisor Tom Arild Blix, who has taught me a lot about rocket and plasma probes. His help, guidance and encouragement has been of great importance for writing this thesis.

I want to thank the people helping me along the way during my work: Martin Friedrich, Markus Rapp and Tore Andre Bekkeng, for providing me with data of other ECOMA instruments that I have use in this thesis, and for their explanations and answers to questions I have asked.

A gratefull thank you also goes to Bjørn Lybekk, who has helped me several times when programs and installations on my computer has failed to work properly.

And, lastly, thanks to Henrike Wilms and Willem de Pous for their encouragement and support during the last phases of this work. It was much appreciated.

Contents

1 Introduction

Every day our atmosphere receives between 10-100 tons of meteoric matter (Hedin et al., 2007). Most of this ablates in the $80-100$ km altitude region (Hunten et al., 1980), forming meteoric smoke particles. It is believed that these small particles play a key role as the nuclei for ice particles, which form noctilucent clouds (NLC) and polar mesospheric radar echoes (see section 2.4). These two phenomena have received an increasing amount of scientific attention the last few decades, due to a possible connection to the detection of climate changes (Friedrich and Rapp, 2009). To date, most of the questions regarding these phenomena are answered, but a few unanswered questions are still subject to ongoing research.

The region of occurrence for the above mentioned phenomena lies within an altitude range that is rather difficult to obtain data from. It is too low for satellites, and too high for balloons to reach, making access to data more scarce than it is for the lower and higher regions. Most ground-based instruments are limited by low time and/or height resolution in the upper mesosphere (Friedrich and Rapp, 2009), apart from some lidars, which, under favorable conditions can measure atmospheric parameters up to about 100 km. Rockets are valuable when it comes to in situ measurements regarding investigation of meteoric aerosol particles. This is because they can provide unique high resolution data from the upper mesosphere.

This thesis focuses on the last of the four rocket campaigns of the ECOMA program (see Table 1). ECOMA is an acronym for "Existence and Charge state Of Meteoric dust particles in the Middle Atmosphere" and was a sounding rocket program aimed at studying meteoric smoke particles in the middle atmosphere (Blix and Hoppe, 2003). All the rocket launches were conducted at Andøya Rocket Range, 69^o N in northern Norway. The main objectives of this program (Rapp, 2011) were to:

- Prove the existence of meteor smoke particles in the middle atmosphere.
- Quantify the concentration of meteoric smoke particles in the middle atmosphere.
- Understand the charging properties of meteoric smoke particles.
- Clarify the role of mesospheric smoke particles (MSP) for the nucleation of mesospheric ice.
- Study MSP evolution during a major meteor shower.

The summer launches took place during different geophysical situations and at different times of the day (two near noon and one near midnight), while the winter launches all took place in the morning hours and at almost the same solar zenith angle (see Table 1). During all three summer flights, the payloads flew through a NLC. Polar mesospheric summer echoes (PMSE) were present only during the first and third launch (Hoppe et al., 2011b).

Table 1: The ECOMA campaigns

Campaign	**Flight**	**Date**	**UT**	**Aim**
ECOMA-2006	ECOMA 1	08.09.06	22:17	Prove existence
	ECOMA 2	17.09.06	21:07	
ECOMA-2007	ECOMA 3	03.08.07	23:22	Relation to NLC/PMSE
ECOMA-2008	ECOMA 4	30.06.08	13:22	Relation to NLC/PMSE
	ECOMA 5	07.07.08	21:24	
	ECOMA 6	12.07.08	10:46	
ECOMA-2010	ECOMA 7	04.12.10	04:21	Effects of major meteor shower
	ECOMA 8	13.12.10	03:24	MSP composition
	ECOMA 9	19.12.10	02:36	

The primary focus of this work is on the last campaign. It was the winter campaign with the flights of ECOMA 7, 8 and 9, that took place in December 2010, before, during and after the peak of the Geminids meteor shower. The main scientific objective of this campaign was to study the effect of enhanced meteor flux in the atmosphere (Rapp, 2011).

The study of meteoric smoke particles is interesting not only because of the possible connection to NLC and PMSE, but also because it modifies the charge balance in the lower ionosphere, and provides surface area for heterogeneous chemistry. It is also a likely form in which meteoric matter reaches the ground (Rapp, 2011).
What I have mainly worked with from this campaign, are analysis of the electron and ion density profiles. During the early preliminary work with these data, a proceedings article (Hoppe et al., 2011c) was written, where I have contributed with data analysis resulting in the figures showing the ion and electron densities profiles from ECOMA 7, 8 and 9. In this thesis, improved analysis of these profiles will be presented.

2 Background

2.1 The Atmosphere

The division of the atmosphere can be seen in two different ways. One way is to define layers based on the temperature profile, another way is to divide the atmosphere according to the mixing mechanisms which can be either winds and large scale convection or diffusion.

In the atmosphere, pressure and density decreases exponentially with increasing height. The atmosphere is divided into different layers, or spheres, by its thermal structure. Generally we say that in each sphere the temperature is either increasing or decreasing with altitude. The place where the temperature reaches a maximum or minimum before changing direction again, is called a pause. Figure 1 shows the averaged thermal structure in the atmosphere for summer and winter at 69^o north. It also shows the different atmospheric layers. The temperature profiles and height of the different atmospheric layers change depending on season and location.

The lowest layer in the atmosphere is the troposphere. Its altitude ranges from the Earths surface up to about 8 km in the polar regions and to about 18 km at the equator. This is the region where most weather phenomenas occur. As we see from Figure 1, the temperature in this region decreases with altitude.

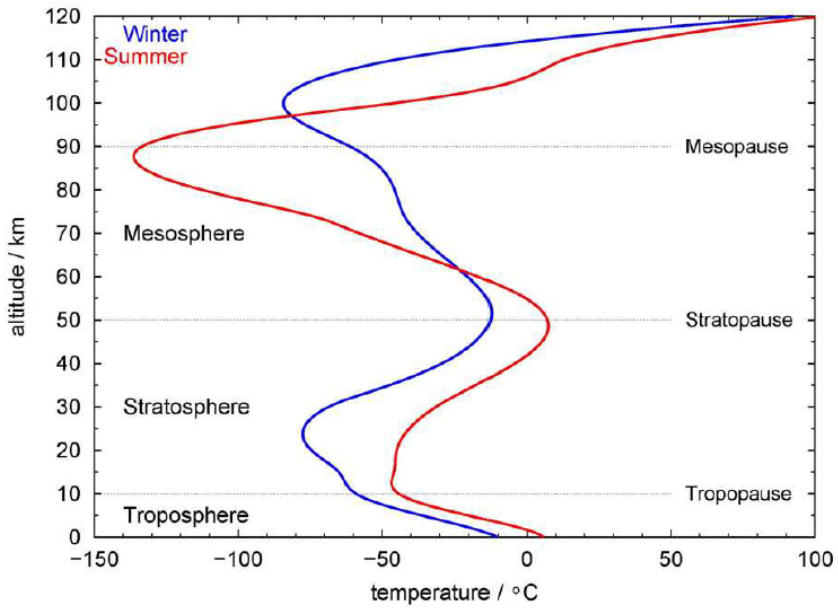

Figure 1: Mean atmospheric temperature profile of summer (red) and winter (blue) at a latitude of 69^{o}N. The dotted lines give a rough indication of the pauses. Data is taken from the CIRA86 model. Figure is from Dunker (2011)

The next layer is the stratosphere. The stratosphere ranges from about $8 - 18$ km, up to about 50 km altitude. It contains the ozone layer, which absorbs most of the high frequency ultraviolet radiation from the sun. The absorption process heats up the air, resulting in an increasing temperature with increasing height. The stratosphere is also the region where Polar Stratospheric Clouds (PSC) form.

Following the stratosphere is the mesosphere. As seen from Figure 1, the height of the mesosphere varies quite a lot from summer to winter. It ranges from roughly 50 km to about 87 km in summer and up to about 100 km during winter at a latitude of 69^{o}N. In the mesosphere, the air density is so low that absorption by solar radiation is not enough to heat up the air, so the temperature decreases with altitude. There is very little water vapor in the mesosphere, but the mesosphere contains higher percentages of ozone than the lower levels. Another important attribute visualized in Figure 1 is that the temperature in the summer polar mesosphere is significantly lower than that of the winter temperature. In fact, according to von Zahn et al. (1996), the temperature in this region can differ as much as 70 K from winter to summer. The reason for this counterintuitive fact is due to a circulation pattern caused by gravity waves. The meridional wind combined with slow vertical adiabatic winds with an upward drift during summer, and downward drift during winter, respectively, giving rise to adiabatic cooling during summer and adiabatic warming during winter.
(for more detailed information see (Dunker, 2011))
Where the mesosphere ends, we find the mesopause. “The thermal structure of the

mesopause region (80 to 20 km) is influenced by a number of complex physical and chemical processes (e.g., radiation processes in non-local-thermodynamic equilibrium, energy exchange between CO_2 an O, dissipating gravity waves, turbulent transport of energy, momentum, and source constituents, energetic particle equilibrium)" (Hoppe et al., 2011c). In the high polar summer mesopause the temperature can drop down to as low as ~ 130 K (Dubietis et al., 2011). The height of the mesopause varies according to seasonal change, and altitude. In the high polar areas, during winter, it can go as high as up to 100 km, while in the summer, it can be around 86 km (von Zahn et al., 1996). The mesosphere/mesopause region is host to a number of interesting phenomena. It is where most meteoric matter ablates, and where phenomena such as PMSE and NLC occurs. This is the region of most interest for this thesis.

The following layer is the thermosphere. In this layer the temperature increases due to absorption of highly energetic radiation. This is the layer where phenomena such as auroras occur in the polar regions. The range of this layer varies due to solar activity, but goes from the mesopause up to several hundred km until its transition to the boundary of space, the exosphere.
What has been described so far was the division of the atmosphere by its temperature profile. As mentioned before, the atmosphere can also be divided by the mixing mechanisms.

The turbopause is located at about 100 km and is the transition region between the homosphere, and the heterosphere. In the homosphere, which is the region below the turbopause, the neutral constituents are mixed by winds and turbulence, so that the composition is almost constant with height. This neutral composition of the gas is as follows; 78% of N_2, 21% of O_2 and the remaining 1% of other constituents. Above the turbopause, in the heterosphere, diffusion is the main "driver", and the chemical composition, dominated by a few atomic or molecular species, varies. Since convective heating is absent in this height, the material in the heterosphere is layered according to its mass. The lower layers are dominated by nitrogen and oxygen molecules, while atomic oxygen is in the next layer, and helium and free hydrogen atoms are prevalent in the region near the boundary of the atmosphere. It should also be mentioned that the lower heterosphere which coincides with the ionosphere also consist of a small area dominated by ionic species or, free radicals such as; O^+, NO^+, O_2^+, N_2^+ and free electrons (APTI, 2011).

It is important to mention that, when looking at a real temperature profile from the atmosphere, the temperature profile does not go smoothly in one direction as it is depicted in Figure 1. Instead, local temperature fluctuations such as depicted by the black line in Figure 11 and 13 are real. This is due to winds and and gravity waves in the atmosphere (Fritts and Alexander, 2003).

2.2 The Ionosphere

The ionosphere is the ionized part of the atmosphere. It can be divided into several different layers defined by the electron density. These layers are; D, E, F_1 and F_2 as shown in Figure 2. From this figure we can also see that the magnitude of electron density varies

significantly depending on daytime, night time, solar minimum and solar maximum. The heights of the different layers also vary greatly solar zenith angle and solar and geomagnetic activity. The layer closest to the Earth's surface is the D-layer. The main ionization source in this layer is Lyman-α radiation at a wavelength of 121.6 nm, ionizing nitric oxide (NO). During periods of high solar activity, hard X-rays may also ionize O_2 and N_2. In the absence of direct sunlight, particle precipitation and cosmic rays are the remaining sources of ionization. The height range of the D-layer is not constant, but varies depending on the ionizing sources. It can range from roughly $50 - 60$ km, up to the beginning of the E-layer.

The E-layer has the most stable height range of the ionospheric layers from altitudes roughly between 80/90 km up to about 150 km (Blix. 2011). The ions in this layer are mainly O_2^+ and NO^+ and are mainly ionized by solar X-rays in the $1 - 10$ nm range, and UV-radiation in the $100 - 150$ nm range. (Kivelson and Russel, 1995) The F_1 and F_2 layers are primarily composed of O^+. F_1 has a maximum electrondensity near approximately 170 km. The F_2 layer is at the last layer of the ionosphere. It is also the layer that varies the least in charge density.

It should also be mentioned that there is charge neutrality in the ionosphere, it means that there are just as many positively and negatively charged species present, so that the net charge is zero.

For more specific information about the ionization processes, and more information about the different layers, see Kivelson and Russel (1995).

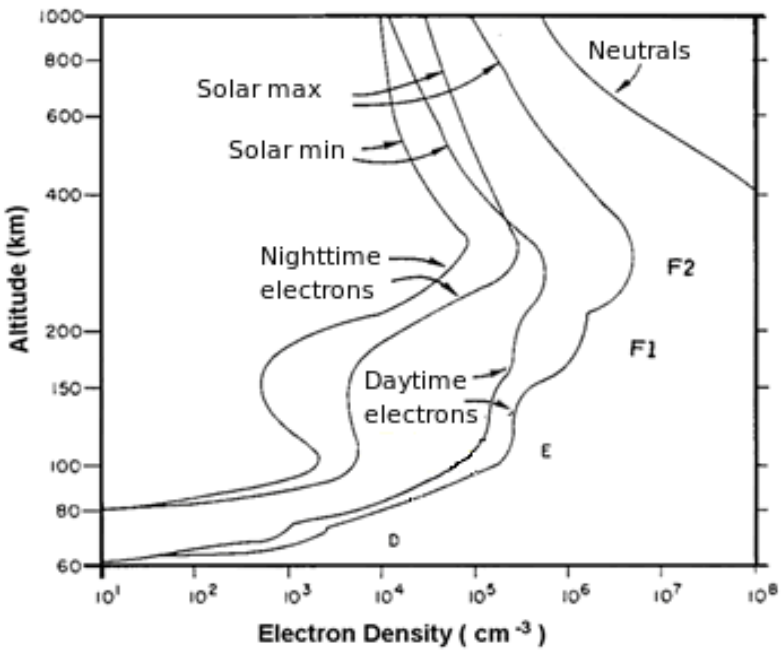

Figure 2: The ionosphere and its layers and typical variations.

2.3 Meteoric Matter

As mentioned in the introduction, our atmosphere is bombarded with $10 - 100$ tons of meteoric matter every day. Most meteors are smaller than a grain of sand, but some can be much greater. The incoming matter is mainly due to sporadic meteors. But a few times during the year, there are major meteor showers. The meteor shower that has the highest meteor flux in the northern polar hemisphere is the Geminids. Its peak is every year around the 13th of December. Most of the meteors entering the atmosphere go through the process shown in Figure 3. As it enters the atmosphere, frictional heating by the increasingly dense atmosphere results in meteoric ablation, mostly in the upper homosphere region between $80 - 100$ km (Hunten et al., 1980). When ablated, it is in the form of atoms and molecules. After ablation, the meteoric residual recondenses and coagulates to smoke particles. The smoke particles sediments in the atmosphere, where heavier particles tend to reach lower heights than light particles. These particles are believed to be an important nuclei in the formation of ice particles that result in NLC and PMSE in the mesospheric region.

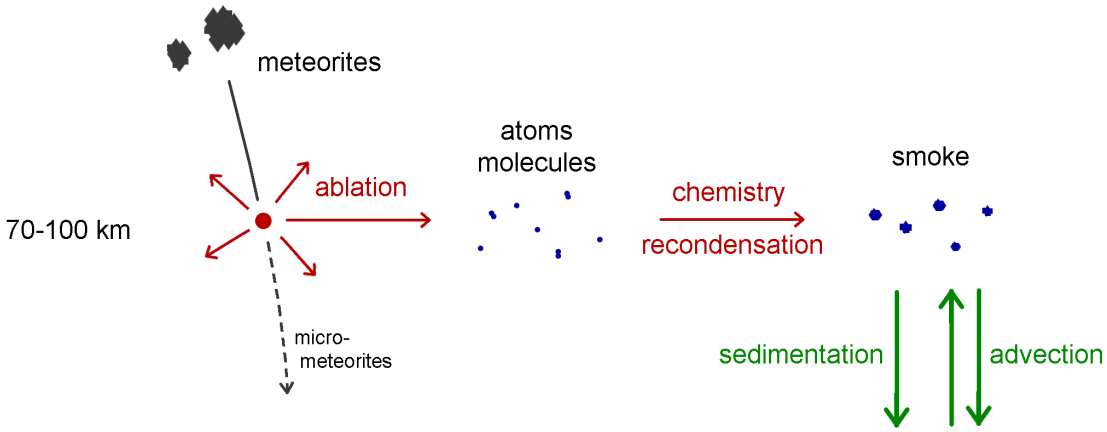

Figure 3: Meteoric ablation process.

Since the ECOMA Geminids campaign studies the increase of meteoric particles flux during the Geminids meteor shower, I will shortly include a description of it.

The composition of the meteors in the Geminids shower is different from other meteor showers. Normally meteor showers are caused by debris streams created by comets and their tails. But, the object creating the specific debris associated with the Geminids, is not a dusty, icy comet, but a rocky asteroid called Phaethon 3200. This asteroid is different from other asteroids crossing the Earth's orbit. It passes closer to the sun and has a different color, suggesting a different composition to most asteroids. The interesting part is that meteoric particles from the Geminids are more solid than meteorids known to come from comets. The first few meteors from the Geminids was detected in the early 1060's, but the first estimate of the strength of the Geminids came in 1877, when the hourly rate was given as about 14. Since then the intensity and amount of meteors in the shower keeps increasing. Today, the peak of the hourly rate is about 80. (Physorg, 2011), (Online, 2011)

2.4 PMSE and NLC

Polar Mesospheric Summer Echoes (PMSE) are strong radar echoes mainly observed by radars in the VHF wavelength. It is generally accepted that these echoes are due to heavy charged aerosol particles with radii $\sim 5 - 50\,\text{nm}$, that reduce the diffusion of free electrons due to ambipolar forces (Rapp et al., 2003). Figure 4 shows a time-height display of PMSE. As is the case in the figure, PMSE normally occur in the altitude range between about $80 - 90\,\text{km}$, close to the cold summer mesopause between late May to mid August in the northern hemisphere. For a review about PMSE see Rapp and Lubken (2004). When the ice particles are in great numbers, and also generally grow to sizes ranging from ~ 20 to $150\,\text{nm}$, they can be detected as Noctilucent Clouds (NLC).

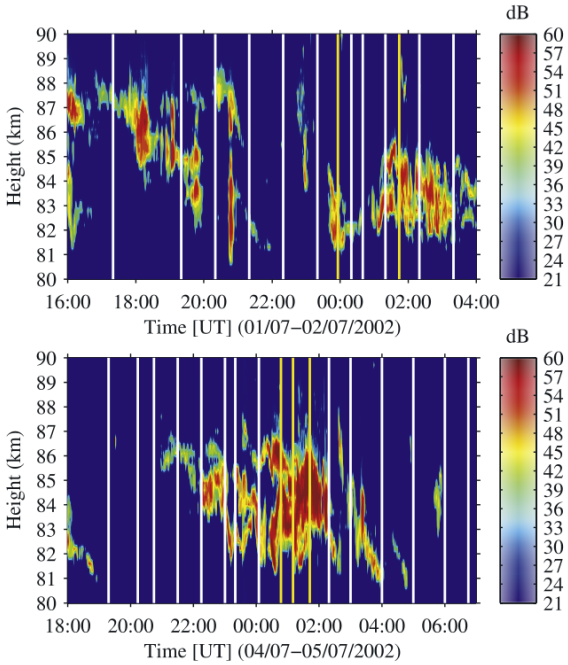

Figure 4: Time-height displays of PMSE intensity showing the variability in PMSE and the various rocket measurement times during the two summer MaCWAVE/MIDAS (Goldberg et al., 2004).

Noctilucent clouds (NLC), depicted in Figure 5, is a cloud-like phenomena that has only been observed since 1885. It was then attributed to having a connection to a volcanic eruption of Krakatoa that occurred two years earlier. Whether or not this phenomena existed before this, is unknown. NLC form right below the mesopause typically around an altitude of $83 - 84\,\mathrm{km}$, just below the cold summer mesopause. The phenomena can be observed from ground in the summer months in mid latitude regions of 50^o to 60^o latitude (Dubietis et al., 2011). The only time they can be observed is right after sunset when the sun is between $6 - 16^o$ below the horizon (Avaste, 1993), when the sunlight still illuminates the upper mesosphere, and the rays of light are scattered in the clouds. That the cloud is illuminated on an otherwise dark sky, is what has given the phenomenon its name (meaning "night-shining").

For NLC particles to form, enough water vapor in the otherwise dry mesosphere is crucial. Another crucial part of the formation is the presence of condensation nuclei. It is now generally believed that meteoric smoke particles may be the most abundant nucleation particle (other, less abundant particles may be water cluster ions). Also the temperature has to be sufficiently low, typically below $150\,\mathrm{K}$ (Murray and Plane, 2005), to permit ice crystal formation. When these criteria are persent, ice can condensate on the aerosol particles, grow in size, be detected by radars as PMSE, and then possibly be observed as NLC at slightly lower altitude than the previous PMSE.

Figure 5: Noctilucent clouds with a herring structure in Finland. Picture: SPL (2011).

It should also be mentioned that there seems to be an increasing number of observations and brightness of NLC. This is one of the reasons why some scientist believe the occurrence of these clouds may have something to do with climate change.

For more information about NLC, see Rapp et al. (2003) and Avaste (1993).

3 Instrumentation During the ECOMA Campaign

3.1 Payload instrumentation

The following sections will describe some of the instruments that were part of the ECOMA payload. I have chosen only to describe the instruments that I use data from in this work. The instruments that will not be described further here, but were also part of the ECOMA payload, were the NO-Photometers developed by the Department of Meteorology at Stockholm University (MISU), and the Pirani gauges developed by the Leibniz-Institute of Atmospheric Physics (IAP). The instruments that I will describe in the following sections are:

- The Positive Ion Probe and Forward Electron Probe developed through a cooperation between the Norwegian Defence Research Establishment (FFI) and the Technical university of Graz (TUG).
- The Multi-Needle Langmuir Probe System (m-NLP) developed at the University of Oslo (UiO).
- The Faraday Experiment (TUG).
- The CONE instrument developed through a cooperation between IAP and FFI.
- The ECOMA Particle detector developed at IAP.

There were three launches of two payloads during the ECOMA Geminids campaign. This means that the payload on ECOMA 7 was recovered, refurbished and used again on ECOMA 9. Figure 6 shows the front deck of the payload and Figure 7 shows the CONE instrument, which was at the rear deck. For a schematic overview of the placement and orientation of the different instruments, see Figure 8.

It should be mentioned (Chung et al., 1975) that "Electric-probe theory is complicated because probes are boundaries to plasmas, and near boundaries the equations that govern the plasma behavior change. Charge neutrality does not hold near boundaries; a thin layer exists where electron- and ion-number densities differ, and the layer, often called a Debye sheath, can sustain large electric fields".

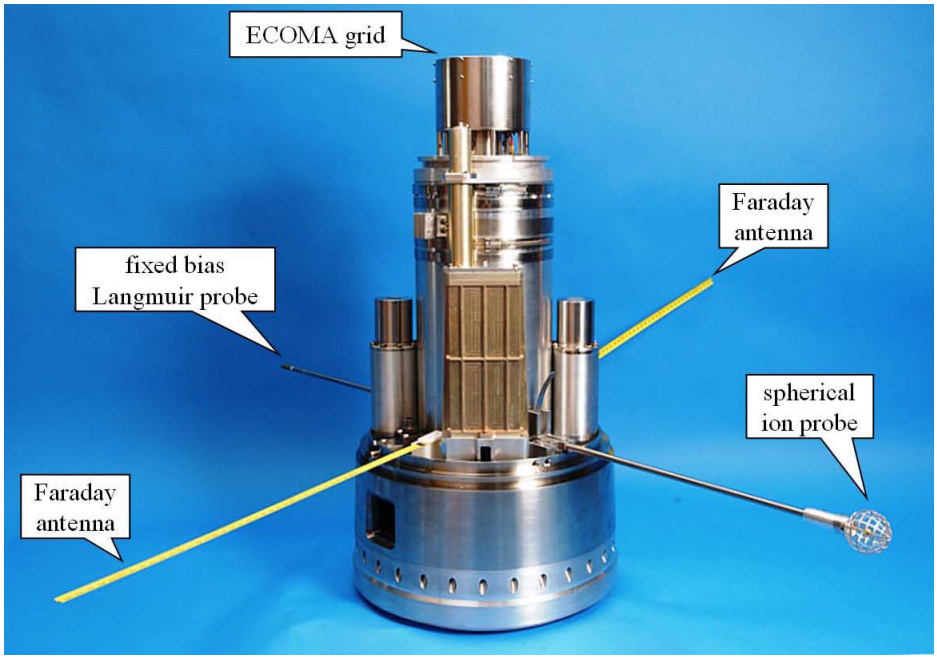

Figure 6: Image of the front deck of the paylad (Hoppe et al., 2011a)

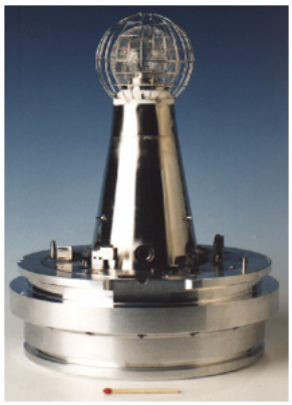

Figure 7: Image of the CONE instrument (Rapp, 2011)

The descriptions of the following instruments are heavily based on information from the Flight Requirements Plan for the ECOMA Campaign 2010 (FRP, 2010).

3.1.1 Positive Ion Probe (PIP) and Forward Electron Probe (FEP)

The PIP is a gridded sphere with a fixed −2.5 V negatively biased collector, while the FEP is a cylindrical probe with a fixed 2.5 V positively biased collector. They measure positive and negative current with 16 bit resolution, proportional to the density of positive ions and electrons (respectively), the rocket velocity and the probe cross section. They are designed to have a high height resolution of less than 1 m, and measure the fine structure in the upper mesosphere and lower thermosphere. (FRP, 2010) and (Blix, 1988) PIP has a radius of 25 mm and FEP has a radius of 1 mm and a length of 25 mm. See also Szuszczewicz (1972) and (Friedrich and Rapp, 2009) for principles behind probes like FEP.

3.1.2 Multi-Needle Langmuir Probe System (m-NLP)

"The goal of the probe system is to record absolute electron density variations along the rocket trajectory with a high sampling rate. The experiment has four identical cylindrical probes with a radius of 0.51 mm and a length of 25 mm. The probes are biased at a fixed potential, equally spaced between 2.5 V and 5 V. The collected current from each probe is then simultaneously sampled with 16 bit resolution, and the electron density is calculated post flight. Two probes are mounted on each of the two booms in the aft section of the payload. Although two probes would be sufficient to calculate the electron density, four probes are utilised to ensure redundancy" (FRP, 2010). For more information regarding the m-NLP, see Bekkeng (2009).

3.1.3 Faraday Experiment

Linearly polarized HF waves change their polarization due to the total electron content between the ground-based transmitter and the rocket payload (Faraday rotation). The electron profile is obtained due to differentiation with respect to altitude. Four frequencies were used to assure good sensitivity at low altitudes on the one hand, and coverage up to apogee on the other(FRP, 2010). The resulting electron density profile is the one we attach most credibility to since its absolute values are insensitive to payload charging and aerodynamic effects. However, the height resolution is usually not better than 1 km, which was the case for the ECOMA winter campaign. For more detailed information, see FRP (2010) and Friedrich et al. (2011).

3.1.4 ECOMA Instrument (Particle detector)

The following description is taken from FRP (2010).
The particle detector applied for the current study is a combination of a Faraday-cup and a Xenon-flash lamp for the photo-ionization of meteor smoke particles. The design of the Faraday cup is similar to the one described in Havnes et al. (1996). It comprises a collector electrode for the measurement of particles of either positive or negative charge, and two grids biased at +/- 3.0 V relative to payload potential to shield the collector electrode from electrons and ions. The flash lamp is operated at a repetition rate of 20 Hz. Immediately after the flash, the charge detected at the collector electrode is recorded for 48 samples at a rate of 100 kHz. After a flight time of less than 1 ms, the detector (which moves at

a typical speed of $500 - 1000\,\mathrm{m/s}$) has passed through the actively ionized atmospheric volume. It then records naturally charged particles reaching the collector electrode at a sampling rate of 1 kHz, until the whole sequence starts again after 50 ms (FRP, 2010).
Hedin et al. (2007) point out that particle detectors on rockets face major challenges due to aerodynamics. The small smoke particles tend to follow the gas flow around the payload rather than reaching the detector. They also conclude that "The flow through a ventilated detector has to be relatively large in order to significantly improve the detection efficiency" (Hedin et al., 2007).

3.1.5 CONE instrument

The description of the CONE instrument is taken from (FRP, 2010).
"CONE (COmbined measurement of Neutrals and Electrons) is a classical triode type ionization gauge optimized for a pressure range between 10^{-5} t 1 mbar, thus suitable to measure absolute neutral air number densities in an altitude range between $70-120\,\mathrm{km}$. In order to obtain absolute densities the gauges are calibrated in the laboratory using a high quality pressure sensor like a Baratron. CONE consists of spherical electrode grids of high transparency, without being surrounded by any structure. This allows the air molecules to stream 'through' the sensor. The main purpose of the CONE design is to reduce the instrumental time constant thus enhancing the ability to resolve turbulent neutral air density fluctuations at spatial scales as small as 1 m. In addition to the triode-system, CONE possesses two more electrodes: While the outermost grid is biased to +2.5V to measure electrons at high spatial resolution (also better than 1 m), the next-inner grid (-15V) is meant to shield the ionization gauge from the ionospheric plasma." This instrument is depicted in Figure 7.

3.1.6 Rocket configuration

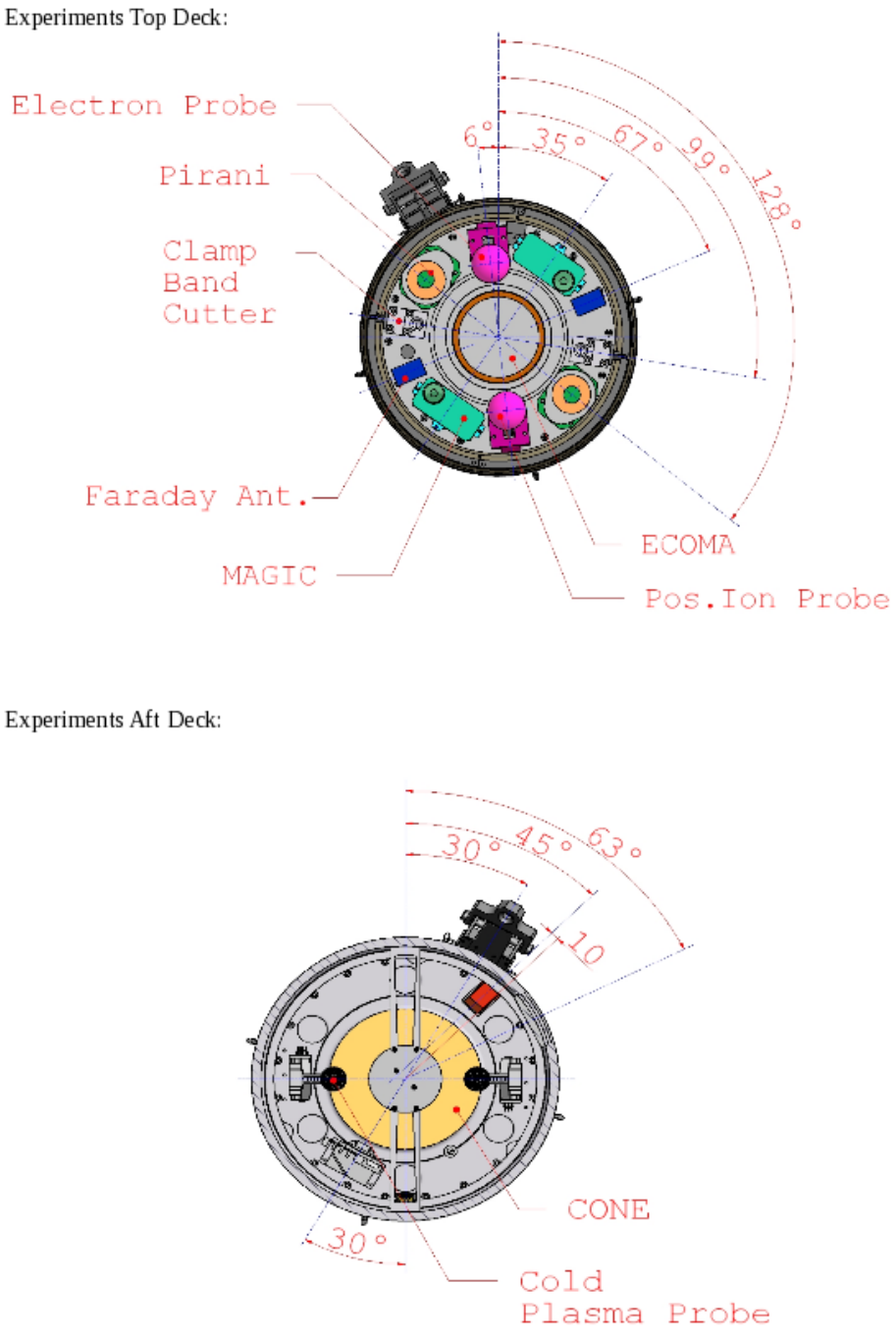

Figure 8: Orientation diagram of payload (FRP, 2010)

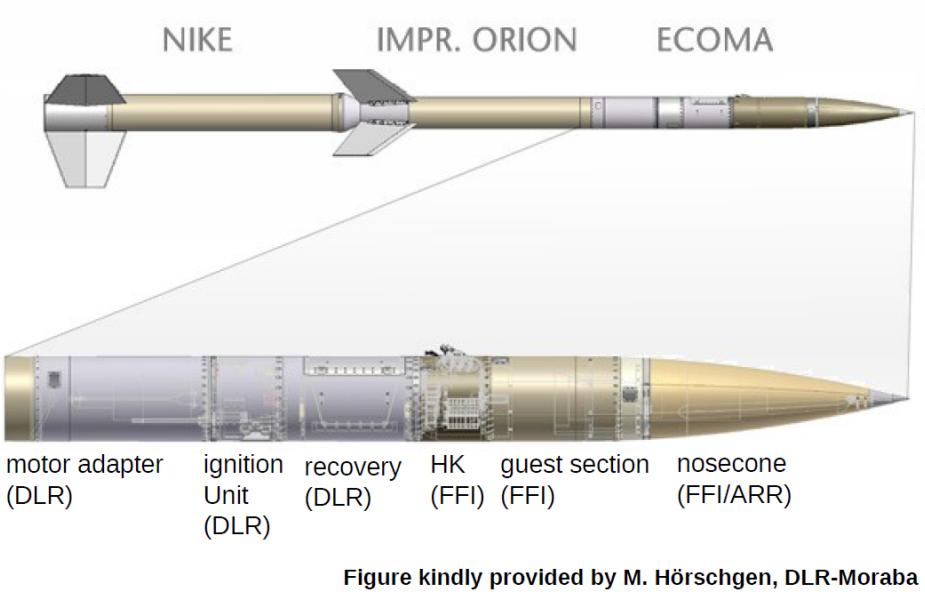

Figure 9: Composition of the rocket

3.2 Ground-based instruments

During the winter ECOMA campaign, there were several ground-based instruments under operation. The following list from Rapp (2011) lists what instruments, and the type of information they can obtain, in the order of their importance during countdown:

- Meteor radar; measure meteor trail echoes.
- EISCAT; measure electron densities and meteor smoke parameters from spectra.
- MAARSY-Radar; measure meteor head echoes.
- ALOMAR Na-lidar; measure wind, temperature and Na density.
- ALOMAR RMR-Lidar; measure wind and temperature.

Of these instruments, I have only directly used data from the Na-Lidar, hence, a short description is given in section 3.2.1.

3.2.1 Na-Lidar

This section is mainly based on information from Dunker (2011).
The sodium lidar is located at ALOMAR (Arctic Lidar Observatory for Middle Atmosphere Research) which is part of the Andøya Rocket Range. The lidar is Co-owned by the Colorado State University, Colorado Research Associates, UiO and Andøya Rocket Range. Lidar is an acronym for "light detection and ranging". In the case of the sodium lidar,

light is scattered by resonance fluorescence from sodium atoms in the mesopause region. This means that "if the emitted photon of a laser has a frequency of one of the allowed transitions from the ground state of the scatterer, the photon will be resonantly absorbed." After the absorption the excited state may relax to a lower state (or the ground state) and emit a photon. If the photon relax on a level above the ground state, this process of absorption and emission is called fluorescence. The backscattering spectrum of Na is sensitive to temperature, so the Na lidar obtains temperature measurements from the Doppler broadening of the backscattered signal from the sodium atoms.

The Na lidar can only be under operation when there is a clear sky and no daylight.
For more detailed information on how lidars work, and how other parameters are obtained, see Dunker (2011).

4 Data and Data Analysis

For better comparison ability I have only focused on the upleg data in this work. To demonstrate the difference in the measurements from upleg and downleg, Figure 10 has been included. This figure shows measurements made by m-NLP on ECOMA 7 on both upleg and downleg. It demonstrates how much the electron density can change over a horizontal distance of several tens of km. If I had more time, and the problems concerning the analysis of some of the downleg data (e.g. from the backward electron probe electron density measurements) were solved, analysis of the downleg data could also have been interesting to present here.

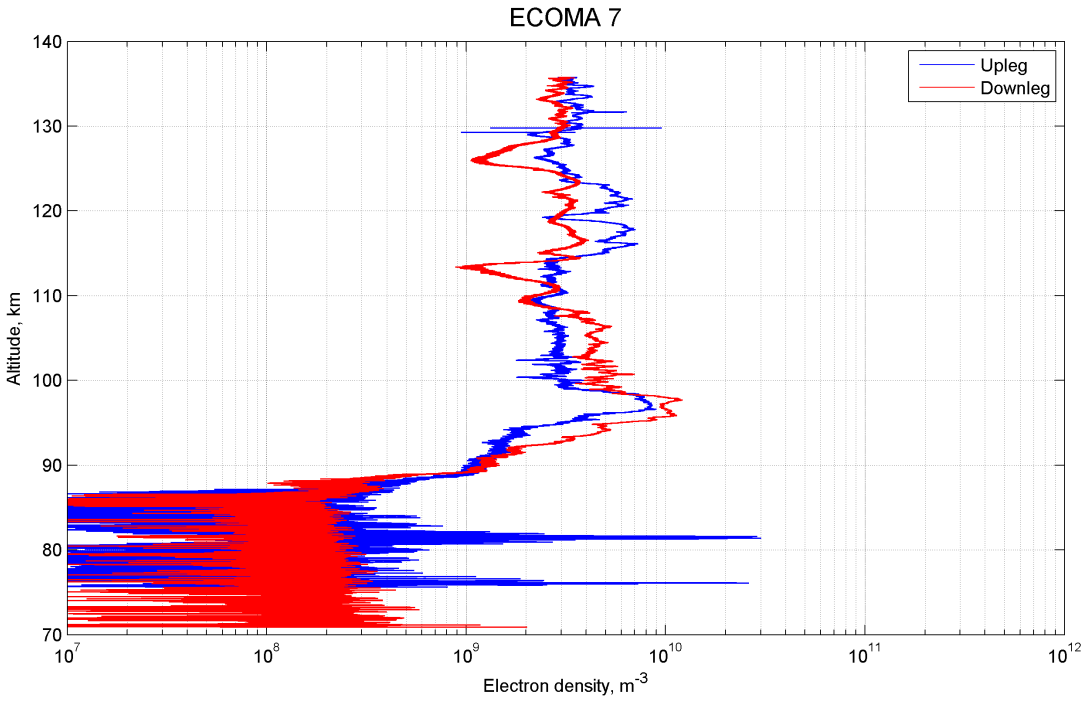

Figure 10: Electron density measured by m-NLP on upleg (blue) and downleg (red).

4.1 From Raw Data to Final Profiles

The following four sections will present how the raw data of FEP and PIP results in the final electron and ion density profiles. This includes the formulas used to calculate charge density, removal of spin, removal of noise and normalization of charge density profiles. In the fifth section a comparison of different measurements from the ECOMA Geminidis campaign will be presented and discussed.

4.2 Calculation of Charge Density

The equations presented in this section are taken from Blix (1988) and Folkestad (1970).

The Positive Ion Probe (PIP) and the Forward Electron Probe (FEP) measured currents. To be able to calculate the charge densities from such measurements, we need an expression relating the measured ion current (I_i) to the ion density (N_i), shown in equation (1), and an expression relating the measured electron current (I_e) to the electron density (N_e) given by equation (2).

$$N_i = \frac{I_i}{\pi {r_0}^2 e v_{ti} [\frac{1}{2}\exp(-x^2) + \sqrt{\pi}(\frac{x}{2} + \frac{1}{4x}\mathrm{erf}(x))]} F_i(U) \tag{1}$$

$$N_e = \frac{I_e}{\sigma_g e v_{te}} F_e(U) \tag{2}$$

The meaning of the constants and variables used in the formulas in this chapter are given in the following table:

Symbol		Explanation
e	-	Elementary charge
$\mathrm{erf}(x)$	-	Error function, see equation (5)
$F_e(U)$	-	Correction function for electron probe
$F_i(U)$	-	Correction function for ion probe
I_e	-	Electron current
I_i	-	Ion current
k	-	Boltzmann constant
m_e	-	Electron mass
m_i	-	Ion mass
N_i	-	Ion density
N_e	-	Electron density
r_o	-	Radius of the spherical ion probe
σ_g	-	Surface of the cylindrical electron probe
T_e	-	Electron temperature
T_i	-	Ion temperature
U	-	Payload potential
v_R	-	Rocket velocity
v_{te}	-	Thermal electron velocity
v_{ti}	-	Thermal ion velocity
x	-	factor, see equation (3)

Both these expressions ((1) and (2)) are related by a correction factor given by the function $F_{i,e}(U)$ due to the charging of the payload. Finding an exact expression for $F_{i,e}(U)$ is very hard, because it depends on the specific payload configuration and charging properties of the rocket that the probe was on. The general agreement among experts is that it must

be dependent on the platform potential U. In practice, $F_{i,e}(U)$ is used as a normalization factor where the calculated densities are normalized to the absolute electron density profile obtained from the Faraday experiment. This is because the Faraday measurements are unaffected by both payload charging and wake effects, and gives the profile we attach most credibility to (Hoppe et al., 2011c). The normalization is done at the height of 99 km for ECOMA 7, at about 90 km for ECOMA 8, and about 91 km for ECOMA 9. Table 2 shows the normalization factors for these flights for the FEP and PIP. See section 4.5 for details on the choice of normalization altitude.

Table 2: Normalization factors

Flight	Instrument	Height [km]	Normalization Factor
ECOMA 7	FEP	99	1.29
ECOMA 7	PIP	99	0.38
ECOMA 8	FEP	90	3.05
ECOMA 8	PIP	90	0.45
ECOMA 9	FEP	91	12.23
ECOMA 9	PIP	91	0.4

Furthermore, the factor x can be written as:

$$x = \frac{2v_R}{\sqrt{\pi} v_{ti}} \tag{3}$$

The thermal velocity of ions and electrons are given by:

$$v_{ti,e} = \sqrt{\frac{8kT_{i,e}}{\pi m_{i,e}}} \tag{4}$$

In equation (1), $\mathrm{erf}(x)$ is an error function dependent on the thermal velocity of ions (see equation (5)). When the thermal velocity is several times lower than the rocket velocity, a simpler equation for the ion density can be used. Considering that the thermal velocity of the ions in the altitude range of interest is about $250 - 400$ m/s, and the rocket velocity is $750 - 1000$ m/s, we see that that the term including the errorfunction in equation (1) can be neglected. We also see that the first term in the parentheses can be neglected too. Inserting the expression for the factor x in the remaining expression in the parentheses, gives equation (6). The condition for this simpler equation holds for at least the altitude range up to 110km for the ECOMA 7,8 and 9 flights, because of the high Mach number. The region of interest in this report is mainly from $80 - 105$ km, so ion densities will not be calculated for regions higher than this, but if ion densities are to be calculated for entire rocket trajectories, the complete expression in equation (1) should be used.

$$\mathrm{erf}(x) = \frac{2}{\sqrt{\pi}} \int_0^x e^{-r^2} \, \mathrm{d}r \tag{5}$$

$$N_i = \frac{I_i}{\pi r_o^2 e v_R} F_i(U) \tag{6}$$

From equation (6), we see that the calculation of ion density is dependent on the rocket velocity v_R, because ions move relatively slow compared to the payload, so that slightly more or less ions will be caught by the probe, depending on the velocity it moves with. Electrons, on the other hand, move with a thermal velocity between $75000 - 105000\,\mathrm{m/s}$ in the region we are looking at. This is so fast relative to the rocket velocity, that compared to the electrons, the payload is barely moving. Hence v_R is not included in the expression of the electron density. This being said, there is another factor that plays a greater role in the calculation of electron density, which is not as significant in the calculation of ion density, namely, the temperature. The electrons move faster with higher temperatures and will more easily collide with the rocket when this is the case. In the next subsection we will take a look at the use of different temperature profiles in the electron density calculations.

4.3 Dependence of Derived Electron Density Profiles on the Temperature Profile

The ion and electron temperature $T_{i,e}$ in the middle atmosphere is assumed to be the same as the neutral temperature in the same region, due to thermal equilibrium.

In this thesis, plots will mainly show results from the $80 - 105\,\mathrm{km}$ height region. As mentioned earlier, it is rather difficult to obtain detailed measurements for this region unless rockets are used for in situ measurements. For the ECOMA winter campaign, an in situ temperature profile from the CONE instrument was successfully obtained only from ECOMA 9. Thus, other temperature profiles had to be used for the other flights when calculating the electron density profiles. When ECOMA 8 was launched, lidar measurements were made simultaneously. The lidar measurements gave a temperature profile in an area close the rocket. Even though this profile may deviate slightly from the temperature in the volume of the rocket trajectory, because of gravity waves (see Fritts and Alexander (2003) for more information) and local differences, it is probably the best temperature profile we can use for our purposes. When no local measurements of temperature is available, as is the case for ECOMA 7, an average standard temperature profile should be used. Such a profile can be found in Lübken and von Zahn (2001). Their paper presents average temperature profiles over Andenes for 9 months, mainly based on lidar measurements but also some in situ measurements.

The discrepancy between the electron density profiles derived from the different temperature profiles shown in Figure 11 is demonstrated in Figure 12. The result is noticeable, but not significant compared to other uncertainties related to e.g. the changing of platform potential. The largest difference between the two temperature profiles is 40K at about 78km, where an electron density calculated on basis of the CONE temperature profile deviates about 4.5% from the density based on the averaged temperature. Since this is outside our region of interest, we can conclude that the two electron profiles deviate less than 4.5% in the interesting region.

Figure 13 shows a plot of the temperature profile obtained from the sodium lidar measurements during the launch of ECOMA 8 (black line). Due to the height of the sodium layer at the time of the launch, a temperature profile could only be obtained from about

83-100km. Since this covers the most interesting region for our purposes, this profile has been used where it provides data, and the standard averaged temperature profile has been used in the ares where we lack lidar data. Since the density profiles will be normalized to the Faraday experiment, the most important attribute of the temperature profile is the variations and structural differences with height, hence, the lidar profile has been shifted by -20 K to fit the averaged temperature profile (dashed line in Figure 13). This was done, so that there would not be a big temperature difference in the area where the temperature profile from the lidar ends and the temperature profile from Lübken and von Zahn (2001) continues.

The conclusion for this matter is that it is best to use temperature profiles that are as close to the true value as possible, but that using an averaged profile only gives a discrepancy of a few percentages, which for our purposes is acceptable.

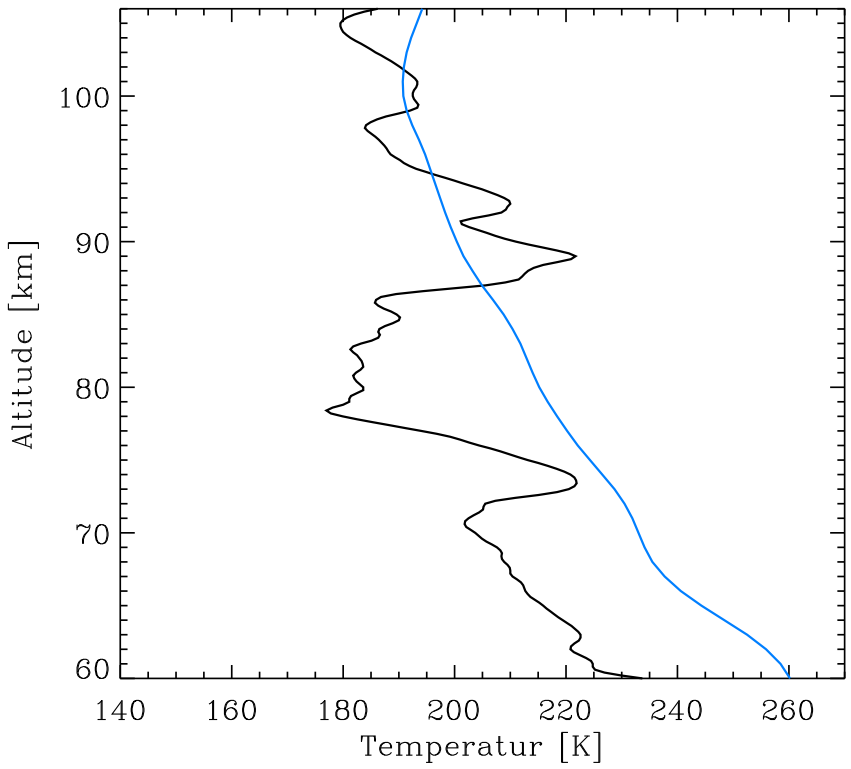

Figure 11: The black line is the temperature obtained from the CONE instrument on the payload on ECOMA 9, while the blue line is an average temperature profile for December, over Andenes taken from Lübken and von Zahn (2001)

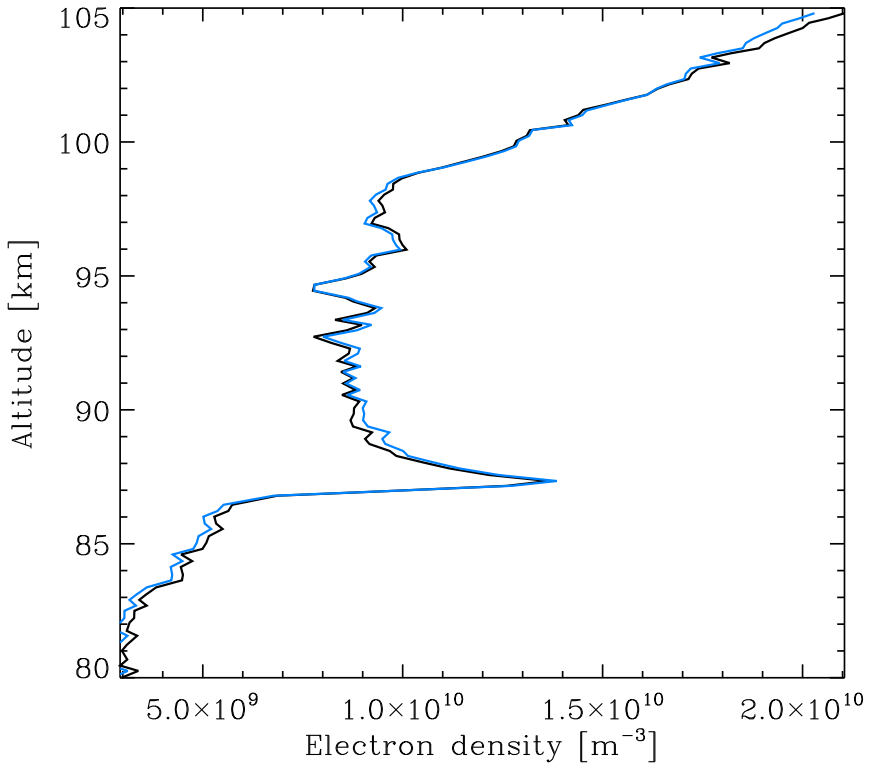

Figure 12: The black line is electron density calculated by using the temperature profile obtained by the CONE instrument on ECOMA 9, the blue line is electron density calculated by using the averaged December temperature profile over Andenes from (Lübken and von Zahn, 2001).

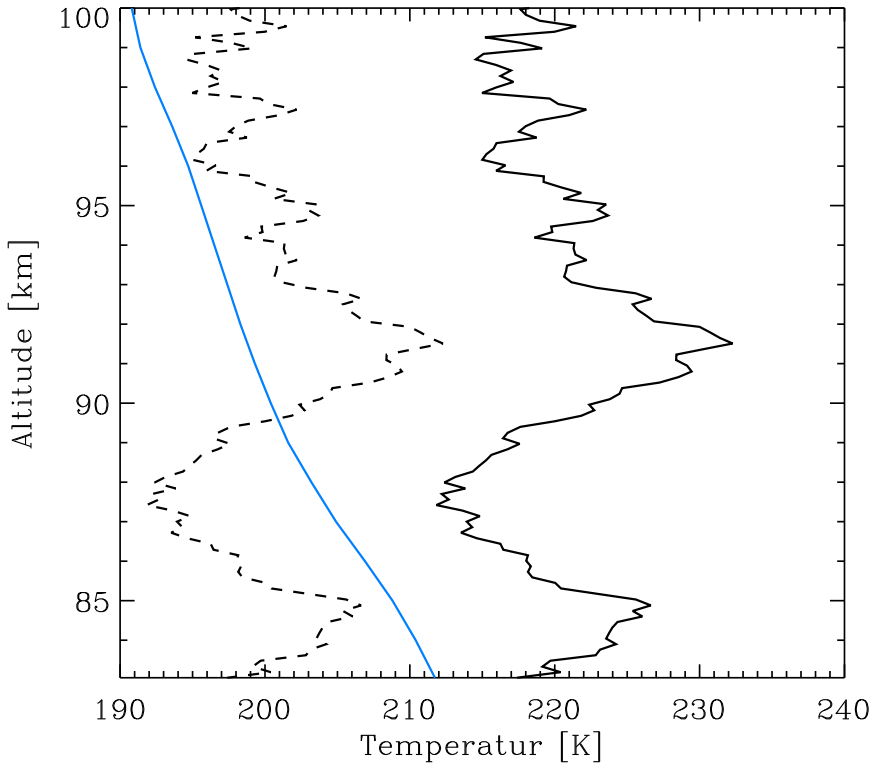

Figure 13: The blue line is an average temperature profile for December over Andenes taken from (Lübken and von Zahn, 2001). The black line is lidar temperature measurements from Andøya, and the black dashed line is the same, but shifted by $-20\,\mathrm{K}$ to align better with the average temperature profile.

4.4 Removal of Spin Modulation and Noise

Sounding rockets are launched with a spin so that they keep a stable direction and orientation during flight. When the rocket moves fast through the gas in the atmosphere, a wake forms around it. FEP and PIP were placed on booms so that they would come outside this wake, but, because of the angle of the rocket, the wake was not uniform around the payload and FEP and PIP spun in and out of the wake. This is why the data retrieved from the rocket measurements were highly effected by spin modulation (see black line in Figure 14). Unfortunately, removing the spin modulation turned out to be a difficult task because the frequency of the spin continuously changed during the flight. For this work, the maximum value of each spin period has been assumed to be the value obtained when the probe is outside the wake, and hence, the correct value. A programming routine was made to find these values, and in that way make profiles without spin modulation. An example of the resulting profile is shown as the red line in Figure 14. (For information on

filtering techniques, see Blix (1988))

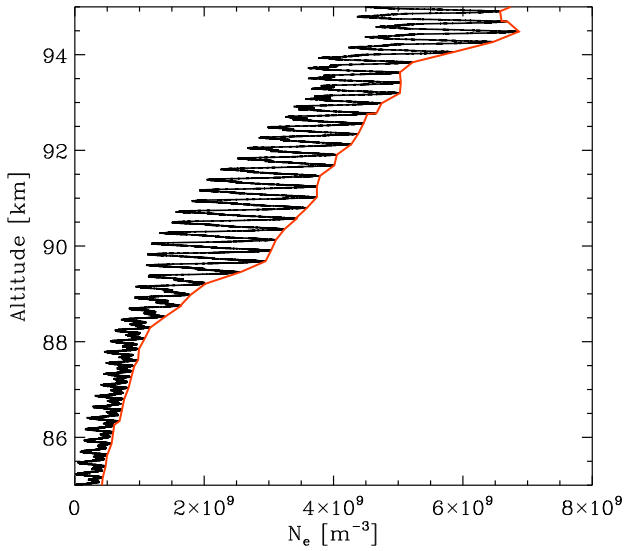

Figure 14: Black line shows spin modulation in the analyzed data from ECOMA 8, red line is made based on the maximum values of each spin.

Another task to perform, when the removal of the spin modulation was done, was to remove the unreliable data contaminated with too much noise. Due to noise, there are no sensible measurements made on upleg by the FEP, PIP and m-NLP before the boom deployment of the m-NLP. The m-NLP boom deployment occurred at an altitude of about $82 - 83$ km for the three flights. For ECOMA 7, the charge density under about 86 km was less then $10^8\,\mathrm{m}^{-3}$. These values are very low for the D-region, and were close to the threshold of what the instruments could detect, hence, there is only noise in these measurements up to about 86 km for FEP and 87 km for PIP for ECOMA 7. Charge densities were higher during ECOMA 8 and 9, so for those flights the noise is only a limit until after the deployment of the m-NLP booms.

The need of normalizing charge density profiles has already been mentioned in section 4.2. What was not mentioned there, was that the electron density profile obtained with the m-NLP also was normalized to the profile obtained by the Faraday experiment. Allthought the m-NLP also measures absolute electron density, it differed from the density profiles obtained by Faraday with about a factor of two. At this time, this discrepancy is attributed to wake effects near the payload (Hoppe et al., 2011c). Work on the physical reasons for this unexpected discrepancy is ongoing.

4.5 Comparison of Different Measurements from the ECOMA Geminids Campaign

All data in this section are from the ECOMA Geminids campaign of December 2010.
The aim of this campaign was to study how the enhanced flux of meteoric matter affects the atmosphere, and to investigate the effect it has on the charge balance in the ionosphere. The launch times for this campaign are listed in Table 3. They were all at night time and at similar solar zenith angle (Hoppe et al., 2011c). The aim was to get the background conditions as similar as possible for all three flights, leaving the meteor flux the only variable.

Table 3: The three launches during Geminidis, 2010 (Hoppe et al., 2011a).

Flight	**Date**	**UT**	**Apogee**	**Conditions**
ECOMA 7	04.12.2010	04:21	135 km	Before Geminids; Smallest electron density ever measured by rocket
ECOMA 8	13.12.2010	03:24	138 km	Geminids maximum; aurora near horizon
ECOMA 9	19.12.2010	02:36	136 km	After Geminids maximum; quiet ionosphere

Figure 15 shows the results from the particle detector for the three flights during the Geminidis campaign. It is assumed that the particles detected are meteoric smoke particles. The smallest particles, with radii less than $2-3\,\mathrm{nm}$ will mostly not be detected by the particle detector, but follow the gas flow around it (Hedin et al., 2007) and (Rapp et al., 2009).

ECOMA 7 and 9 flew an improved version of the ECOMA particle detector with three flash lamps that operated with three different wavelengths, while on ECOMA 8 the old configuration with only one flash lamp was used. The reason for this was that the improved ECOMA instrument had to be refurbished from the first flight on ECOMA7, while this was done, ECOMA 8 flew with an older version of the ECOMA instrument. At the time of the launch of ECOMA 9, the improved ECOMA instrument was done being refurbished, and was used on ECOMA 9.

Figure 15 shows something that looks like positively charged aerosol particles above the negatively charged particles. This may not be the case. According to Rapp (2011) the only geophysically reliable signal from this instrument is the region with negative charge number densities. The remaining positive excursions are remnants of not completely removed contaminations from positive ions.

At the moment, a paper analyzing the results shown if Figure 15 is in the process of being written. What can be seen from just looking at the different profiles from the different flights in this figure is that, before the onset of the Geminids, when only sporadic meteors

ablated in the atmosphere, the smoke particles seemed to be distributed over a rather high altitude range ($83-95\,\mathrm{km}$). While at the peak of the Geminids, the layer of such particles were lower in altitude ($83-89\,\mathrm{km}$) and had higher charge number densities. Before this campaign, it was believed that the profiles of the charged number density of the smoke particles would be approximately the same in the profiles obtained before and after the peak of the Geminids. As we see from the figure, this does not seem to be the case. A few days after the peak, the height region of charged smoke particles is at slightly lower altitudes($82-87\,\mathrm{km}$), but with less charge number density than at the peak of the meteor storm.

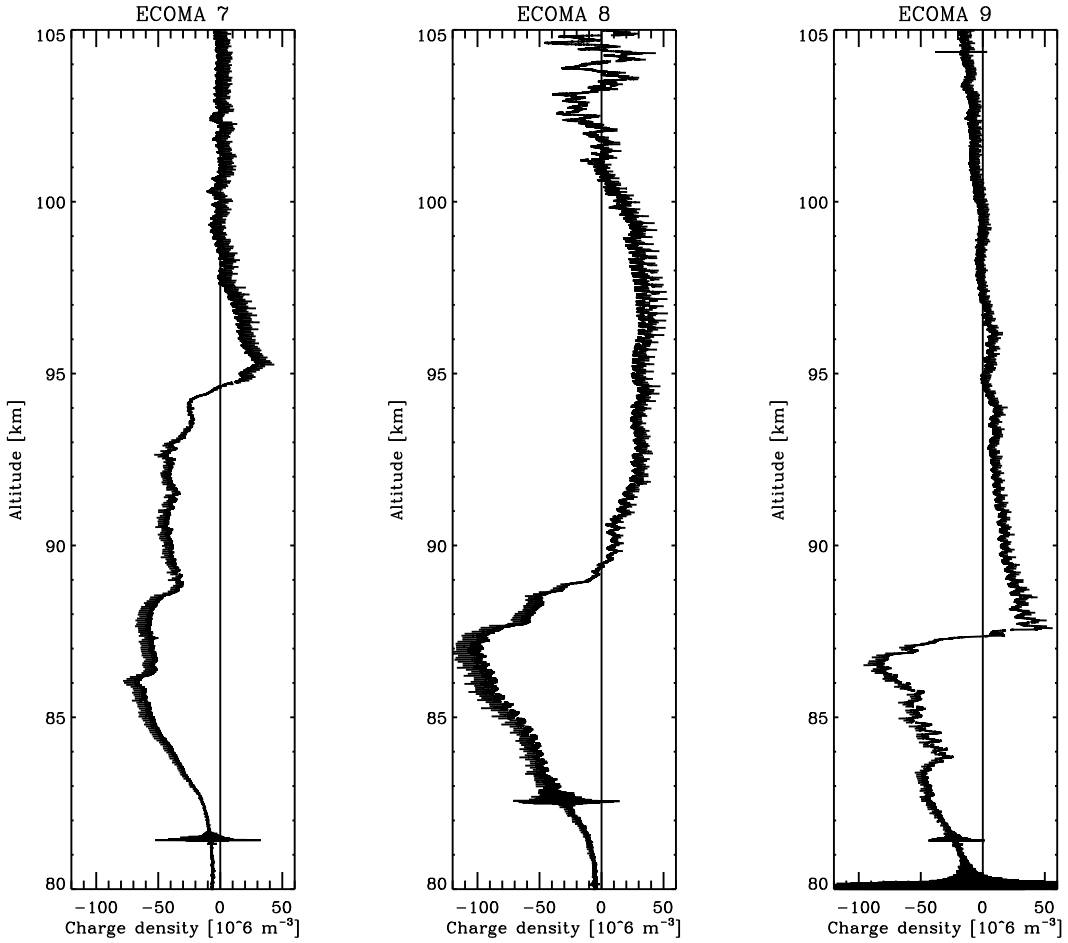

Figure 15: The development of charged aerosol particle densities from the three different flights during the Geminidis campaign. The leftmost is from before the meteor shower, the middle form the peak and the rightmost some days after the peak.

The different electron and ion density profiles, to be presented below, have been normalized to the electron density profile from the Faraday experiment. This is because it is the profile with most credibility. The Faraday profile has a low height resolution but an accurate mea-

surement of absolute electron density. The other instruments give a high height resolution but only a relative value of the charge density. Because of this, the results from these other instruments need to be normalized to the Faraday profile. The normalization heights have been chosen above the area where meteoric smoke particles exist, and in such a way that the profiles overlap as much as possible in the region we are interested in (especially between $80 - 90$ km). The normalization heights have already been presented in Table 2. The heights are not the same for all the flights because of different conditions during the individual launches.

In earlier rocket flights with fewer instruments on each payload, normalizing the electron and ion density profiles from FEP and PIP to the profile obtained by the Faraday experiment would yield a very good and overlapping profile. Nowadays, due to economic concerns, there seems to be a trend of flying more and more instruments at the same time, yielding more complex payload configurations, and resulting in measurements that are more affected by instrumental disturbances. This may be the case with the ECOMA payload, where electron and ion densities do not overlap as well as they used to (Blix. 2011).

In the following three subsections, results from the instruments measuring electron (FEP,m-NLP, Faraday) and ion (PIP) density will be presented and discussed. These results will also be compared to the platform potential obtained from the m-NLP, and the charge number densities of aerosol particle measured by the particle detector.

4.5.1 ECOMA 7

ECOMA 7 was launched before the onset of the Geminids meteor shower. As already mentioned, the charge densities measured by ECOMA 7 are among the lowest densities ever measured by rocket-borne experiments at high latitude. This may not be too surprising considering the conditions under which the launch was conducted. It was night at Arctic winter, meaning an absence of the direct ionizing radiation from the sun. There was also very little geomagnetic activity before and during the launch, leading to very little ionizing particle precipitation. Even the moon, which can have a slight ionizing effect (Friedrich et al., 2010), had a small visible reflective area that night.

The low charge densities were just at the threshold of what FEP, PIP and m-NLP could measure. This is why, as mentioned in section 4.4, there are no electron density profile obtained by m-NLP and FEP below 86 km in Figure 16 and no ion density obtained by PIP below 87 km in Figure 17.

Figure 16 shows the electron density profiles obtained by the FEP, m-NLP and Faraday experiment. As we can see, even though these profiles are normalized in one height (99 km), they do not overlap completely. A small-scale differences between the low resolution electron density profile from Faraday, and the two other high resolution profiles, was expected since FEP and m-NLP detect some small scale structure. A possible reason for the discrepancy of the measurements on the ECOMA flights, may be related to the properties of the varying platform potential (see leftmost plot in Figure 18). This is no surprise remem-

bering the expression (Equation 2) for electron density being dependent on exactly this factor. Another reason may be that the number and complexity of the instruments on the ECOMA payload has disturbed the measurements by FEP and PIP.

Figure 17 shows the electron density profile obtained by the Faraday experiment and the ion profile obtained by PIP. Due to charge neutrality in the ionosphere, there must be as many negatively charged species as there are positively charged species. The positively charged species can be positive ions and positively charged aerosol particles. The negative species can be electrons, negatively charged aerosol particles, and negative ions. The Faraday experiment only measures electrons and not the other two negatively charged species.

In Figure 17, we see that there is a discrepancy between the electron and positive ion density profiles. The ion density seems to be higher than the electron density. This could be due to the before mentioned instrumental reasons or at least partly, due to some of the electrons having been attached to meteoric smoke particles.

Figure 18 shows on the left side, a plot of negatively charged aerosol particles, while the plot in the middle shows the surplus of positive charge by subtracting the electron density from the positive ion density. A plot like that would ideally show the amount of electrons "missing" due to attachment to meteoric smoke particles. As we see, the ions are continuously in surplus where there seems to be meteoric smoke. (The spikes above this region are attributed to the small scale differences due to the different height resolution between the two profiles). The particle detector cannot detect aerosol particles that are (typically) smaller than $2 - 3\,\mathrm{nm}$, electrons can also be attached to some of these smaller particles. It is unknown how many of these small particles there are, nor do we know their height distribution. We also see that the charge density of the positive surplus is roughly a factor 10 greater than the charge density of the smoke particles. This is a big difference, if it was considered exact measurements it could mean that only about 10% of the negatively charged particles would be detected by the ECOMA instrument. But, since we don't know exactly how the PIP has been effected by the payload potential or the other instruments, we cannot draw this conclusion, nor take this number as a real. What we can do is seeing it as a supporting indication of the existance of negatively charged smoke particles, and an indication of there being undetected smoke particles.

It should be mentioned that, at the time of launch, the payload potential is zero, but the moment it gets launched it becomes negatively charged due to the dense atmosphere. If electrons are attached to smoke particles, those otherwise free electrons loose their mobility, and more ions than electrons will collide with the payload, resulting in a decrease of negative platform potential. There seems to be a slight tendency of this in the rightmost plot in Figure 18. This effect is more visible during the ECOMA 8 flight, where there are more meteoric aerosol particles present.

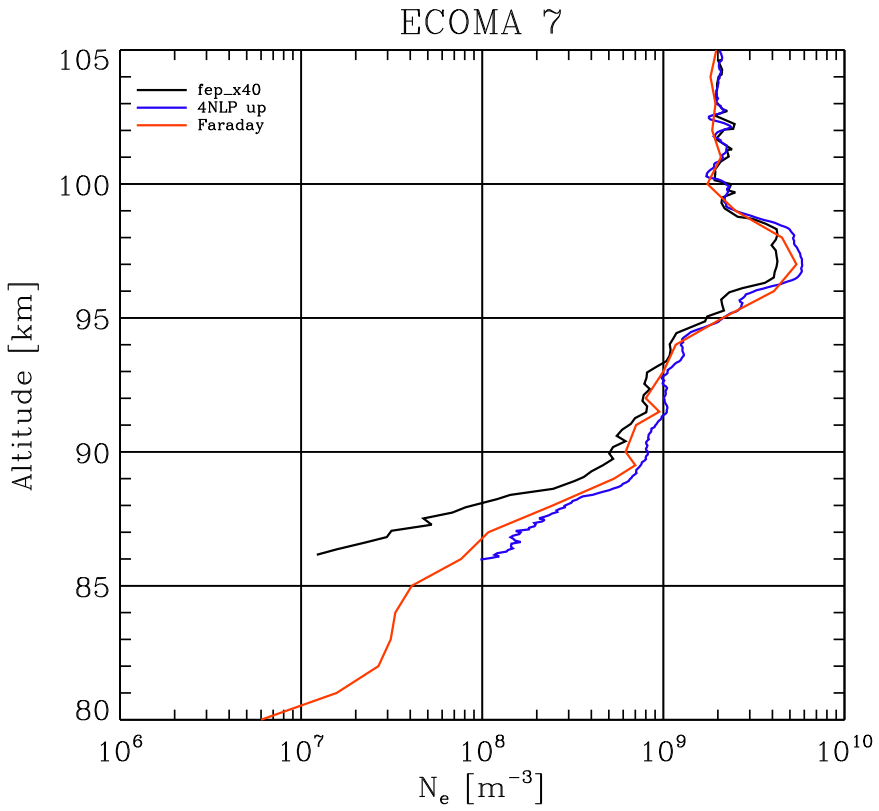

Figure 16: Electron density profiles obtained by FEP (black line), m-NLP (blue line) and the Faraday experiment (red line). Normalized at 99 km.

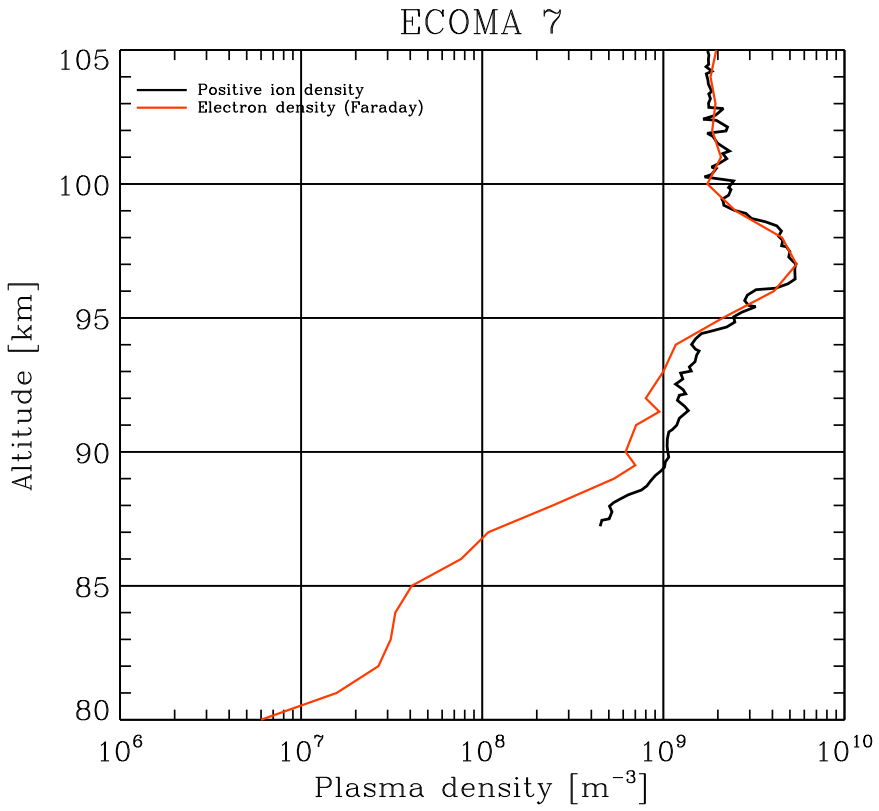

Figure 17: Positive ion density profile obtained by PIP (black line), electron density profile from Faraday (red line). Normalized at 99 km.

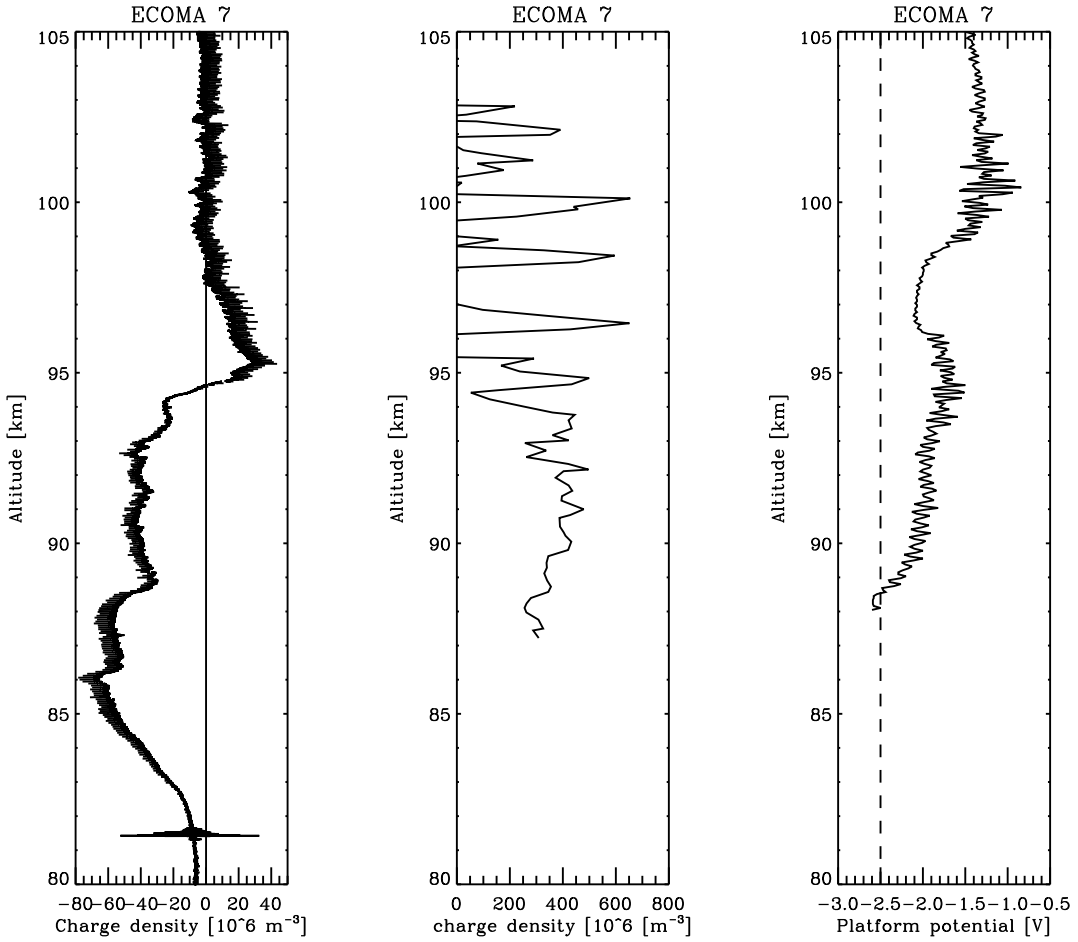

Figure 18: Plot showing, from the left, charged aerosol particle density, the difference between ion and electron density (ion-electron), and platform potential for ECOMA 7.

4.5.2 ECOMA 8

ECOMA 8 was launched at the peak of the Geminids meteor shower. Figure 19 shows an image taken at Andøya the night of the launch, displaying an aurora. It shows that the ionosphere was slightly disturbed this day. This is also reflected from the higher electron and ion densities obtained from the plasmaprobes on the rocket.

Figure 20 shows the electron densities obtained during this flight. The different electron density profiles were normalized at 90 km since the meteoric smoke seemed to be below 89 km. This normalization height gave a relatively good agreement between the profiles in the interesting region under 90 km, but resulted in a noticeably larger discrepancy above this height. Figure 21 shows the electron density profile from the Faraday experiment, and the ion density profile from PIP. These profiles were also normalized at 90 km. It shows a discrepancy both over and under the normalization height, but as seen by comparison with

Figure 22 the discrepancy below the normalization height is in the same height region as there seem to be negatively charged meteoric smoke particles. Figure 22 shows very clearly that the surplus of positive ions is in the same height range as where the smoke particles are. It also shows clearly how the platform potential decreases in this same region. Another explanation for the decreasing negative platform potential than the one mentioned in the previous section, is that smoke particles having a slanting impact on the payload skin can knock out electrons from the payload.

Figure 19: Photo taken at Andøya, 13. December 2010 *Photo: Kolbjørn Blix Dahle.*

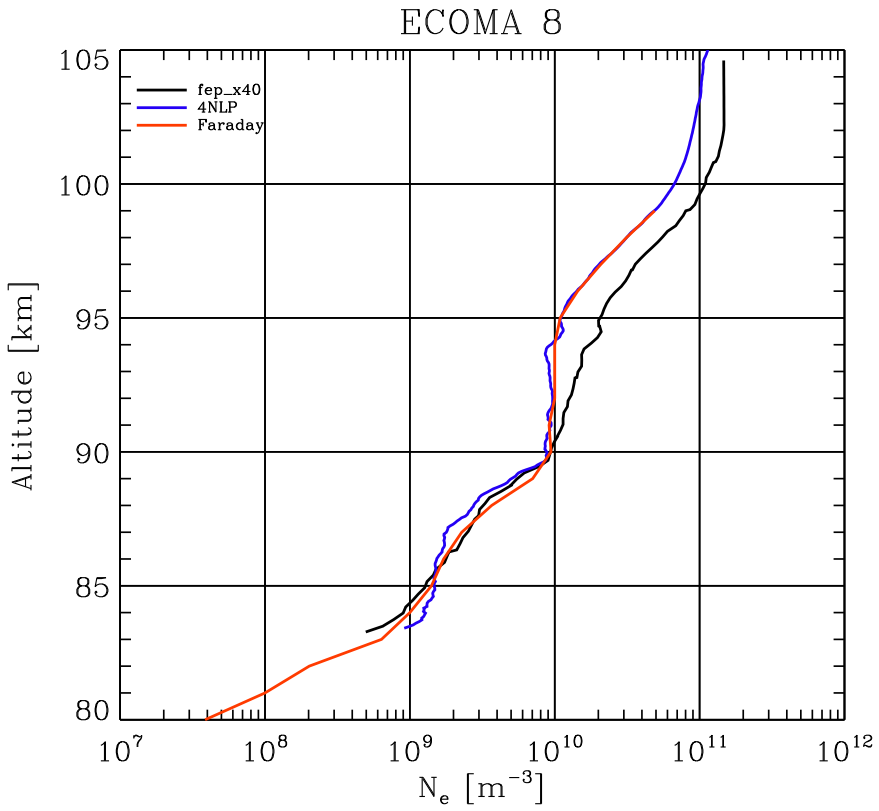

Figure 20: Electron density profiles obtained by FEP (black line), m-NLP (blue line) and the Faraday experiment (red line). Normalized at 90 km.

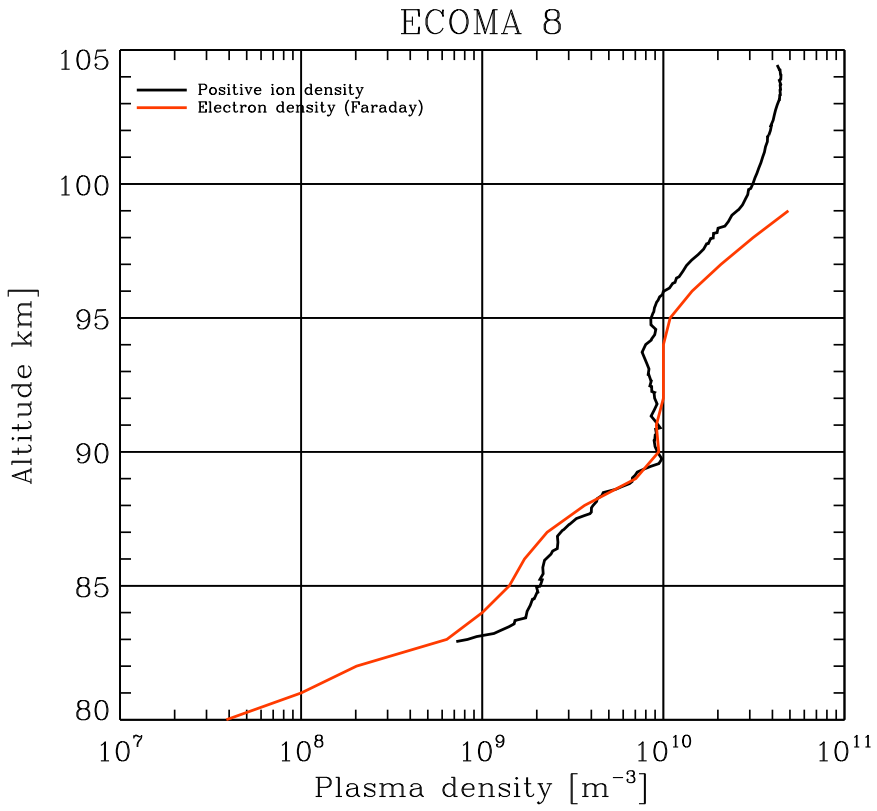

Figure 21: Positive ion density profile obtained by PIP (black line), electron density profile from Faraday (red line). Normalized at 90 km.

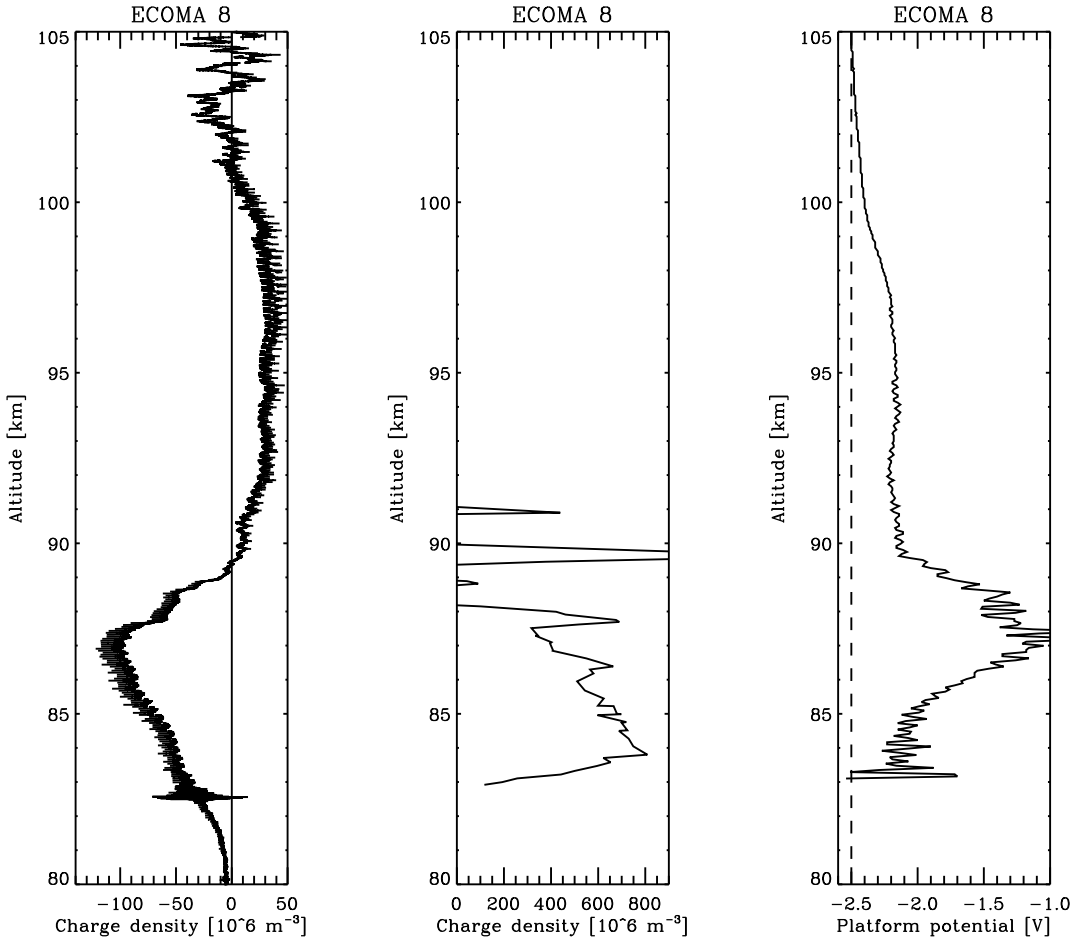

Figure 22: Plot showing, from the left, charged aerosol particle density, the difference between ion and electron density (ion-electron), and platform potential for ECOMA 8.

4.5.3 ECOMA 9

ECOMA 9 was launched a few days after the peak of the Geminids. The ionospheric conditions were more quiet compared to how it was during the launch of ECOMA 8. Figure 23 shows the electron density profiles from m-NLP, FEP and the Faraday experiment. They are normalized in a height of 91 km. The m-NLP measurements overlaps better with the Faraday measurements than the FEP measurements does. This seems to be the case for all three flights. There is a large discrepancy between the electron density profile obtained by FEP, and the two other profiles, both over and under the normalization height. ECOMA 9 has the most negatively charged platform potential of the three winter flights (see leftmost plot in Figure 25) and also the largest discrepancies between FEP and Faraday measurements.

Figure 24 shows the electron density obtained by the Faraday experiment, and the positive

ion density obtained by PIP. The discrepancy between the two profiles under the normalized height may partly be attributed to the attachment of electrons.

Figure 25 shows the same kinds of profiles as Figure 18 and 22 in the previous sections. Also here, the continuous surplus of ions is in the same height range as the negatively charged meteoric aerosol particles. The platform potential shows a slight decrease in potential in the region of the charged smoke particles, in this case too.

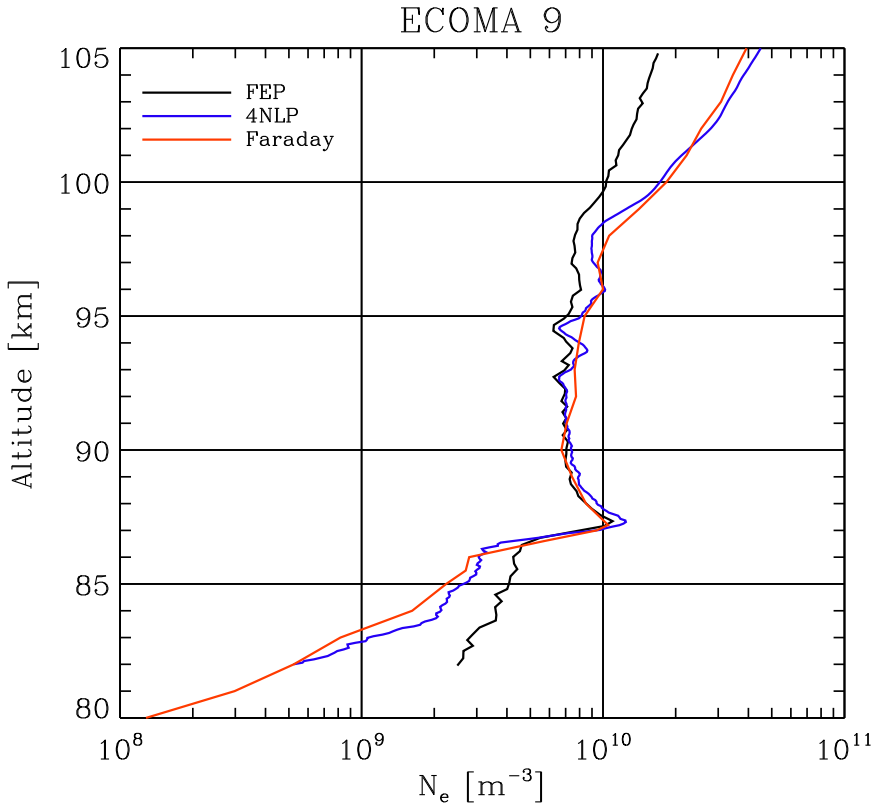

Figure 23: Electron density profiles obtained by FEP (black line), m-NLP (blue line) and the Faraday experiment (red line). Normalized at 91 km.

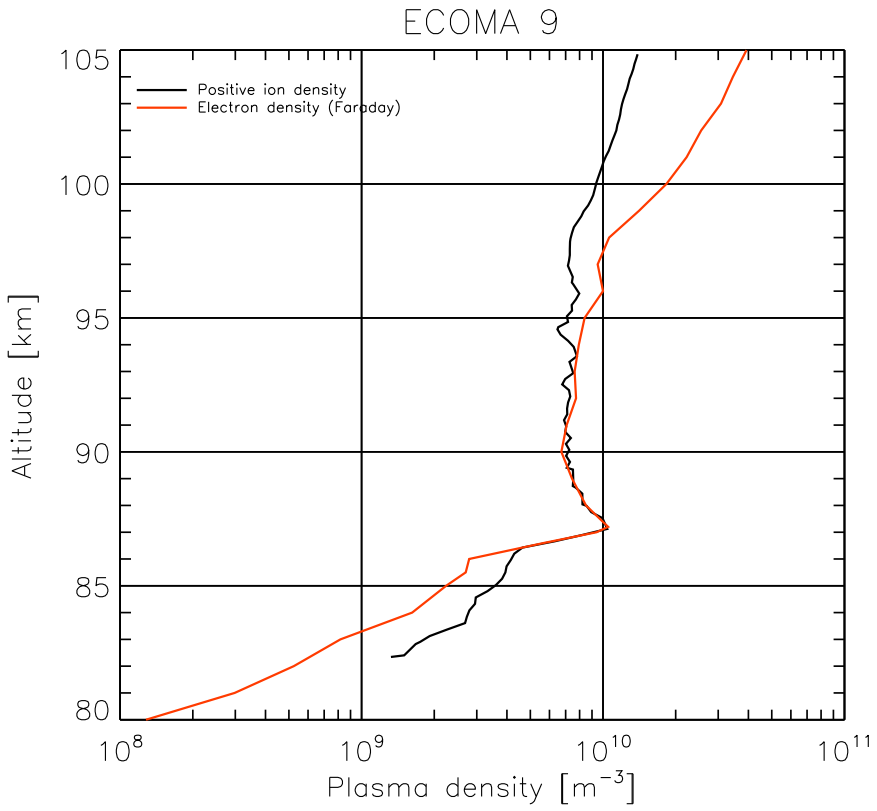

Figure 24: Positive ion density profile obtained by PIP (black line), electron density profile from Faraday (red line). Normalized at 91 km.

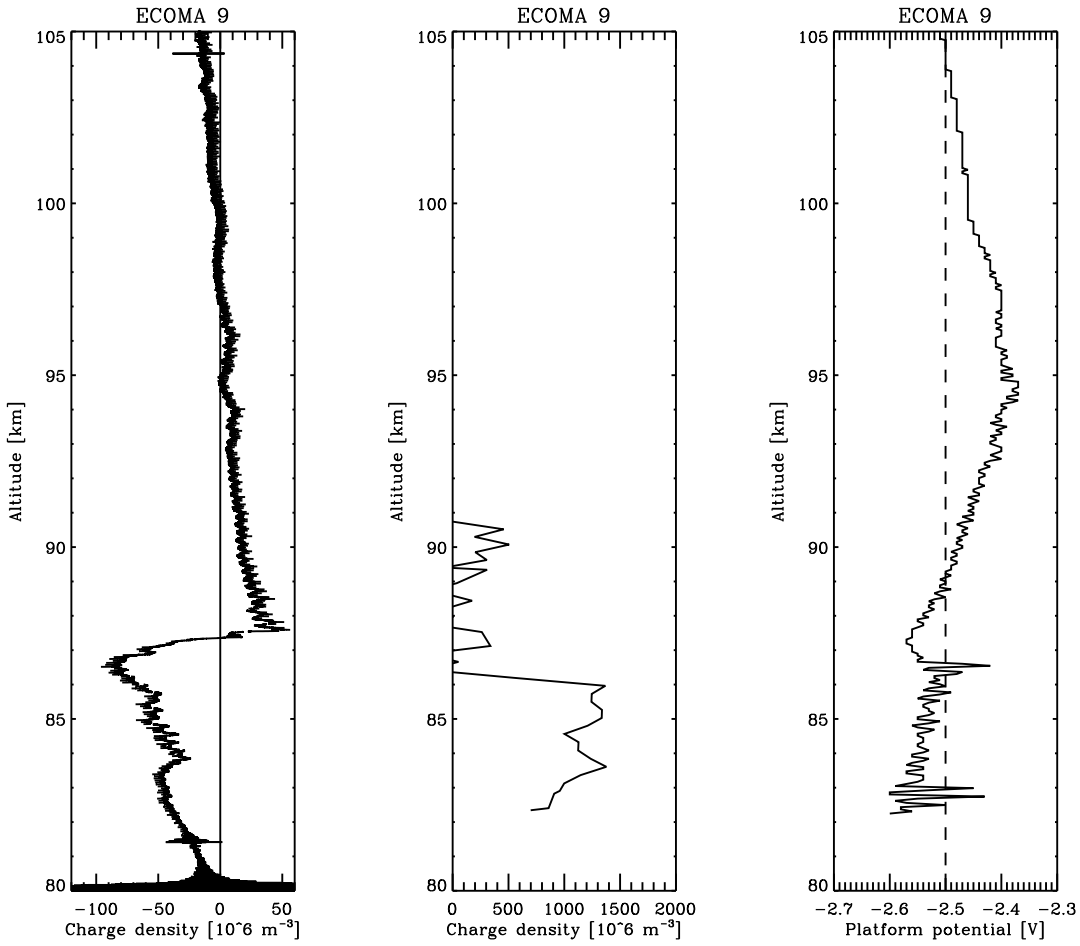

Figure 25: Plot showing, from the left, charged aerosol particle density, the difference between ion and electron density (ion-electron), and platform potential for ECOMA 9.

5 Summary, Conclusion and Outlook

For all three flights during the ECOMA Geminids campaign, a surplus of positive ions were measured with the plasma probes in the region of negatively charged aerosol particles. The aerosol particles are believed to be meteoric smoke particles. Since the otherwise mobile and free electrons are attached to these smoke particles, the surplus of free positive ions would impact the payload, making it less negative when flying through that region. Another possible explanation for the payload becoming less negative when flying through the charged smoke particles, is that the slanting impact of smoke particles on the payload skin knocks off electrons and that way makes it less negative.

A second conclusion is that; due to the magnitude of the large surplus of positive ions, compared with the magnitude of negatively charged aerosol particles, (there was about a factor 10 difference in magnitude), it seems that the ECOMA instrument does not detect all the negatively charged aerosol particles. The factor 10 cannot tell us quantitatively how much is not detected, due to the uncertainties of normalization between charge profiles, but rather serve as a strong indication that there is a large difference.

Due to the relatively good agreement between electron density profiles obtained by m-NLP and the Faraday experiment, and the relatively large discrepancy between these two profiles and the profile obtained with FEP, it is recommended that for later flights, only the m-NLP and Faraday experiment should be used for measuring electron density.

A proceedings article (Hoppe et al., 2011c) (see appendix A), of which I am co-author, treated the early preliminary results of the electron and ion density profiles presented in this thesis. It also compared the payload potential and charged aerosol particles from the ECOMA instrument for ECOMA 8. The conclusions drawn in that article, are in accordance with the conclusions presented above.
Another conclusion from these thesis is that; normalizing electron and ion profiles with the electron profile obtained by the Faraday experiment, should be done in a height above the region where meteoric smoke occurs.
Further work and analysis will be done on the results from the ECOMA Geminids campaign, Appendix B shows a list of 10 upcoming papers, planned to be published in 2012. Of these papers, the ion and electron density profiles that have been worked with in this thesis, may contribute to article number 6,7,8 and 9 in the list in the appendix.

6 Appendix

A Proceedings Article

THE CHARGE BALANCE IN THE PRESENCE OF METEORIC SMOKE IN THE UPPER MESOSPHERE UNDER WINTER CONDITIONS – PRELIMINARY RESULTS

U.-P. Hoppe[1, 2], M. Friedrich[3], T. A. Blix[2, 1], J. I. Moen[1], T. A. Bekkeng[1], K. R. Svenes[2], Å. Svendsen [1], M. Rapp[4], K. Torkar[5]

[1]University of Oslo, P.O. Box 1048 Blindern, N-0316 Oslo, Norway, u.p.hoppe@fys.uio.no

[2]Norwegian Defence Research Establishment (FFI), P.O. Box 25, N-2027 Kjeller, Norway, t.a.blix@fys.uio.no

[3]Graz University of Technology, Inffeldgasse 12, A-8010 Graz, Austria, martin.friedrich@tugraz.at

[4]Leibniz Institute of Atmospheric Physics, Schloßstraße 6, D-18225 Kühlungsborn, Germany, rapp@iap-kborn.de

[5]Space Research Institute, Austrian Academy of Sciences, Schmiedlstraße 6, A-8042 Graz, Austria, klaus.torkar@oeaw.ac.at

ABSTRACT

Three winter flights of ECOMA payloads took place before, during and after the peak of the Geminid meteor shower in 2010 with the aim of studying the effect of an enhanced flux of meteors in the atmosphere. This paper will use data from all the plasma and one particle instruments (ECOMA). We present and comment the performance of the instruments on these three flights and document a clear change of payload potential in the exact height range where negatively charged smoke particles are present.

1. INTRODUCTION

A number of studies underline the importance of understanding the physical, photochemical and radiation processes in the upper atmosphere in order to understand what goes on in the whole atmosphere, including the long-term variations (natural and anthropogenic) that constitute climate variations. A recent study [1] states that both observations and models in the height region 50 to 80 km still are in a state of development, and while the overall agreement of models with observations is encouraging, an improvement of the situation is desirable. The thermal structure of the mesopause region (80 to 120 km) is influenced by a number of complex physical and chemical processes (e.g., radiation processes in non-local-thermodynamic equilibrium, energy exchange between CO_2 an O, dissipating gravity waves, turbulent transport of energy, momentum, and source constituents, energetic particle equilibrium). We need more robust observations of various atmospheric parameters from this height region in order to discriminate the influences of the different processes in a quantitative way and to indentify possible trends [1].

In 2008 and 2010, six ECOMA rocket payloads were launched from Andøya Rocket Range (69˚N) in northern Norway in the periods 30 June – 12 July and 4 – 19 December, respectively. The payloads carried different types of plasma probes to measure positive ions and electrons, as well as a set of particle detectors for measurements of charged and neutral smoke particles and NLC/PMSE particles. Additional on-board instruments measured neutral temperature and density. The summer launches took place during different geophysical situations and at different times of the day (two near noon and one near midnight), while the winter launches all took place in the morning hours and at almost the same solar zenith angle. During all three summer flights, the payloads flew through a noctilucent cloud (NLC); polar mesosphere summer echoes (PMSE) were present only during the first and third launch. All flights were accompanied by a host of active and passive ground-based observations. Many results from the launches in 2008 have been reported in [2] and by eight papers in a special issue prefaced by [3]. The charging properties of meteor smoke and implications for seasonal variation that we have learned in the ECOMA programme have been published in [4]. The processes of electron loss in the presence of meteoric smoke particles have been studied in more detail, using the same flights as this paper, and therefore perhaps in similar preliminary fashion in [5].

In this paper we will concentrate on the performance of the different plasma probes in December 2010 with and without the presence of meteor smoke particles.

2. INSTRUMENTS AND DATA

Of the instruments on board the ECOMA payload, this paper uses the ECOMA instrument [4], the Faraday Experiment [5], the Positive Ion Probe (PIP) and Electron Probe (EP) [6], [7], and the Multi-Needle Langmuir Probe System (m-NLP) [8].

The m-NLP sensors on ECOMA are four identical needles (see Fig. 1) held at four different, small, fixed potentials such as shown for two needles in Fig. 2. It is important that the needle diameter is much smaller than the needle length and that it is much smaller than the Debye length in the target observation height. The braid is kept at the same potential as its needle so that the observation geometry in the plasma is not perturbed from the situation with one long, thin needle (or cylindrical probe) at a given potential. The current is measured from the needles only. The largest m-NLP potential was 5.1 V so as to disturb the other plasma measurements on board as little as possible. The

smallest potential was 2.5 V (both with respect to the payload potential), and the other two equidistant between those two values. When the square of the needle current is plotted as a function of needle potential as in Fig. 2, the slope of the regression line depends only on fundamental constants, the geometric dimensions of the needle and the local electron density [8]. Most importantly, the slope is independent of the payload potential. The intersection of the regression line with the potential axis yields the payload potential.

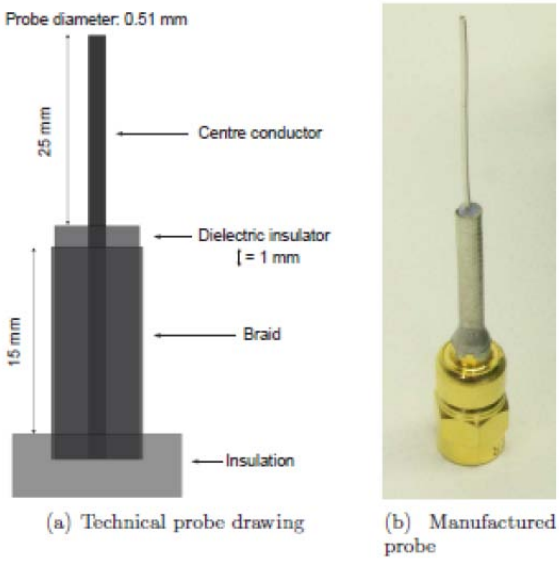

Figure 1. The m-NLP instrument probe [8]

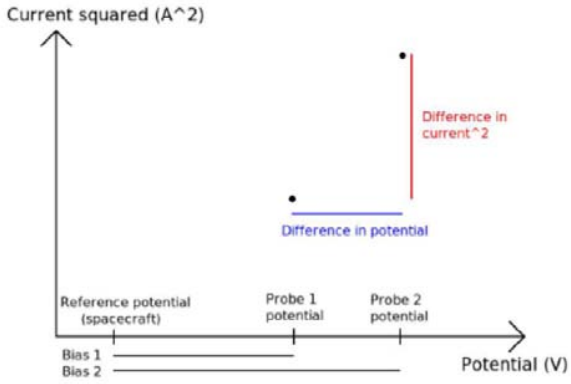

Figure 2. The m-NLP analysis method [8]

Flight	Date	UT	Apogee	Conditions
ECOMA 7	04.12.2010	04:21	135 km	Before Geminids; Smallest electron density ever measured by rocket
ECOMA 8	13.12.2010	03:24	138 km	Geminids maximum; aurora near horizon
ECOMA 9	19.12.2010	02:36	136 km	After Geminids maximum; quiet ionosphere

Table 1. Launch times, apogees, and launch conditions of the three flights presented here. See also [5].

Fig. 3 shows the electron density profile from ECOMA 7. The red line is from the Faraday Experiment, using all usable frequencies, Faraday rotation as well as absorption [5]. It is the profile we attach most credibility to, as it stems from Faraday rotation between the ground-based transmitter and the receivers on the payload. However, it gives only one value per spin rotation period of the payload. To our knowledge, this profile is the lowest electron density profile ever measured by this rocket-borne method at auroral latitudes. The blue and green lines give the corresponding profile measured on upleg and and downleg with the m-NLP completely independently, but on the same payload. Ideally, the red and blue lines should coincide at all heights. Below 86 km, the blue line exhibits interference from the boom deployment and should not have been drawn in this preliminary plot. Also, it would appear that the m-NLP did not perform well at electron densities below 10^8 m^{-3}, a very small electron density for the D-region. Between 86 and 105 km, the values from m-NLP are nearly twice as large as the values from the Faraday experiment. The m-NLP measures the electron density independently of the payload potential, but near the payload. At this time, we attribute the discrepancy to wake effects near the payload, which do not affect the Faraday experiment. Further work is needed to confirm this explanation. The currents measured with the four m-NLP needles are digitally filtered to remove the spin frequency and a large number of higher harmonics before further processing. We will check in the near future how such filtering might 'average' the currents from ram and wake during the spin.

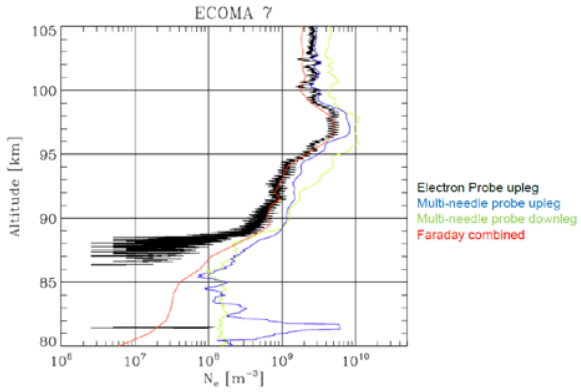

Figure 3. Electron density profiles from ECOMA 7 using three independent instruments, two on upleg and m-NLP both from upleg and downleg. The blue and green lines are unreliable below 86 km.

The green line is the electron density profile from the m-NLP from downleg. It is included to show how much the electron density changes over a horizontal distance of several tens of km. The black line is the electron density profile from the electron probe (EP), which gives a relative value and must be normalised at

one altitude. Here, we have normalised the profile to the Faraday profile at 95 km. This profile still exhibits a strong spin modulation which we did not have time to remove before the ESA Symposium. Below 90 km and above 98 km, the EP profile deviates somewhat from the Faraday profile, presumably due to changes in the instrument's equivalent area in different flow regimes. Experience from earlier flights encourages us that these deviations can be explained by physical processes after further work. Also the EP does not appear to be reliable at electron density values smaller than 10^8 m^{-3}. Note that all three instruments independently detect a small increase between 91 and 92 km, where a sporadic E layer was observed at the same time with the EISCAT radar some 125 km away.

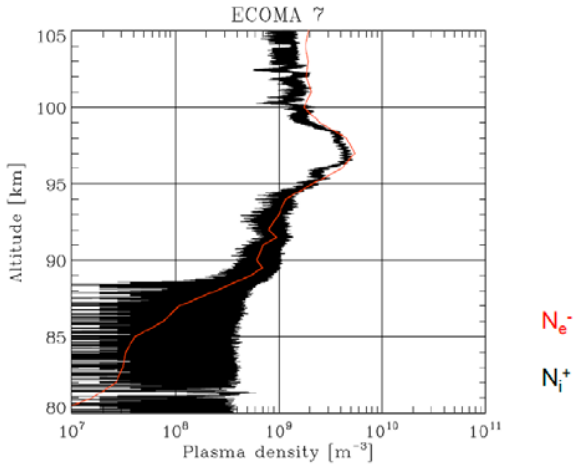

Figure 4. Electron density from the Faraday experiment and positive ion density from PIP on upleg (ECOMA 7)

Fig. 4 compares the red line from Fig. 3 with the positive ion density profile measured with PIP, also on upleg. This profile also needs spin removal before further processing. As EP, PIP gives a relative profile, and we have normalised it to the Faraday profile at 95 km. Also PIP exhibits the small maximum near 97 km. There may be flow and sensitivity issues yet to be studied above 98 km, and the instrument appears to perform unreliably at plasma densities below 10^8 m^{-3}. To the degree of detail visible here, we observe charge neutrality, but see [5].

Fig. 5 is analogous to Fig. 3, but for ECOMA 8. The feature in the m-NLP profile near 82-83 km is an artefact of boom deployment. The m-NLP system shows up to twice as many electrons m^{-3} than the Faraday experiment, presumably due to wake effects. Spin modulation has unfortunately not yey been removed from the EP profile, which was normalised to Faraday at 97 km. In Fig. 6, the spin modulation has not yet been removed from the PIP profile, and it has been normalised to the Faraday Profile at 100 km. We obviously have more work to do concerning the sensitivity of PIP at flows of different velocities.

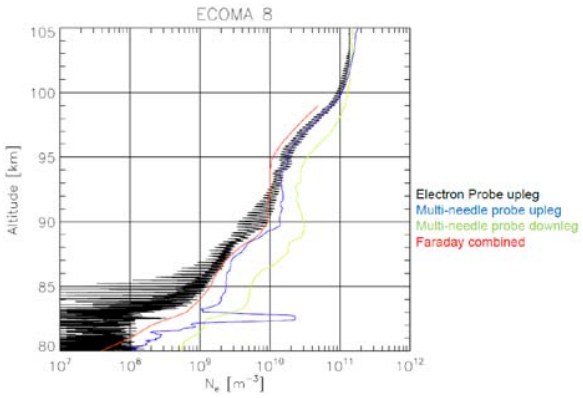

Figure 5. As Fig. 3, but for ECOMA 8

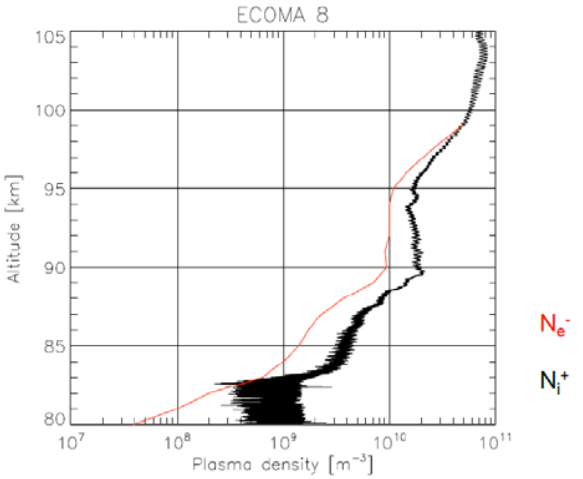

Figure 6. As Fig. 4, but for ECOMA 8

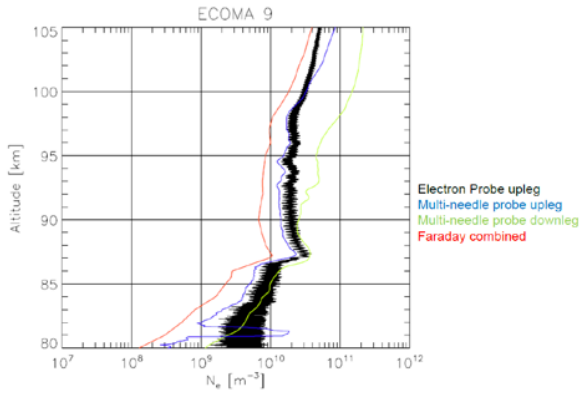

Figure 7. As Fig. 3, but for ECOMA 9

Fig. 7 displays the same kind of data as Fig. 3, but for ECOMA 9. This time, the EP profile has been normalised to the m-NLP profile from upleg at 99 km. The m-NLP profile shows the artefact from boom deployment at 81 km, and perhaps we ought to not have plotted the profile below 82 km. Fig. 8 is analogous to Fig. 4, but for ECOMA 9. The same

general comments apply to Figs. 7 and 8 as to the other pairs.

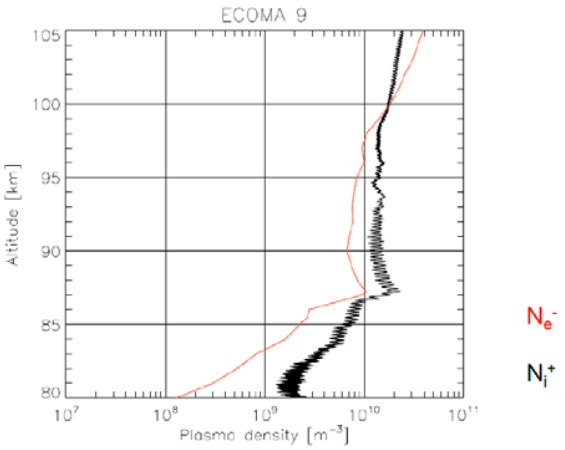

Figure 8. As Fig. 4, but for ECOMA 9. Normalisation altitude 100 km.

Fig. 9 shows in the right panel how the payload potential varied during the ECOMA 8 flight according to the m-NLP. While the payload potential was nearly constant near -2.5 V to -2.6 V, it became much less negative in the height region 85 to 100 km on upleg. We have never had the instrumentation to measure a profile of payload potential at several times during a flight. The left panel of Fig. 9 shows the number density of charged (meteoric) smoke particles from the ECOMA instrument [4]. Obviously, the payload potential excursion happens at the same height where we observe a layer of negatively charged smoke particles, and the two profiles are very similar, even if not exactly mirror images of each other. We observe similar effects on ECOMA 7 and ECOMA 9. Our tentative explanation is that about $8 \cdot 10^7$ m^{-3} of the approximately $2 \cdot 10^9$ m^{-3} negative charges have become attached to smoke particles. Therefore, there are fewer free electrons, which have much larger mobility than smoke particles, and there is correspondingly less negative charging of the payload due to electrons impinging on the payload from all sides. The charged smoke particles collide only with the payload's front deck, a much smaller surface area. Assuming that most of the (meteoric) smoke particles were negatively charged, which we will know after further analysis of the ECOMA data, our observation would also agree with another possible physical process: Glancing collisions of smoke particles on the payload skin could knock out electrons from the payload, thus leading to a smaller negative potential.

3. CONCLUSIONS AND OUTLOOK

As expected, we observed no strong electron bite-outs in December. The payload potential becomes less negative in the presence of meteor smoke particles, either because some of the otherwise free electrons become attached to smoke particles and lose their mobility, or because the slanting impact of smoke particles on the payload skin removes electrons from the payload. The multi-needle probe measures a high-resolution electron density profile in the immediate vicinity of the payload, independent of the payload potential, but presumably these measurements include wake effects. The Faraday experiments measures the electron density profile as the derivative of the total electron density between the transmitter on the ground and the receiver on the moving payload – without wake effects but with coarser height resolution. For future sounding rocket launches, we recommend combining the Faraday experiment, the Multi-Needle Probe and the Positive Ion Probe as a plasma diagnosis package.

This paper shows early, preliminary results from the data analysis after less than six months. Additional work will refine the details of the profiles, hopefully remove spin modulation and yield much more information by combining information with other on-board and ground-based results.

ACKNOWLEDGEMENTS

We thank Stig Karsrud, Terje Angeltveit, Vidar Killingmo, Karsten Holen, and Sven Ivar Holm for excellent technical support, as well as the personnel of DLR MoRaBa. Personnel at Andøya Rocket Range contributed flexible, constructive and pleasant launch services. The Norwegian Space Centre and the Research Council of Norway supported the Norwegian contribution to the ECOMA programme (half of the common costs) with funding under grants 197629 and 191754. The German part was supported by the German Space Agency (DLR) under grants 50 OE 0301 and 50 OE 0801 (Project ECOMA). The Austrian participation in the ECOMA series of rocket flights was made possible through grant 18560 of the Austrian Research Fund (FWF). Against all odds, FFI made possible the final ECOMA campaign.

4. REFERENCES

1. von Zahn, U. & Berger, U. (2011). *Langfristige Änderungen in Eigenschaften der oberen Atmosphäre.* Nordrhein-Westfälische Akademie der Wissenschaften und der Künste, NM478, ISBN 978-3-506-77348-7, Verlag Ferdinand Schöningh, Paderborn, München, Wien, Zürich.

2. Rapp, M. Strelnikova, I., Strelnikov, B., Friedrich, M., Gumbel, J., Hoppe, U.-P., Blix, T. A., Havnes, O., Bracikowski, P., Lynch, K., Knappmiller, S. (2011). Microphysical properties of mesospheric aerosols: An overview of in-situ results from the ECOMA project, in: IAGA Special Sopron Book Series, Vol. 2, *Aeronomy of the Earth's Atmosphere and Ionosphere*, edited by M.A. Abdu, D. Pancheva & A. Bhattacharyya, Springer, ISBN: 978-94-007-0325-4.

3. Rapp, M. & Robertson, S. (2009). ECOMA/MASS: aerosol particles near the polar summer mesopause. *Ann. Geophys.* 27, 823-1456.

4. Rapp, M., Strelnikova, I., Strelnikov, B., Hoffmann, P., Friedrich, M., Gumbel, J., Megner, L., Hoppe, U.-P., Robertson, S., Knappmiller, S., Wolff, M., Marsh, D. R. (2010). Rocket-borne in-situ measurements of meteor smoke: Charging properties and implications for seasonal variation, *J.Geophys.Res.-Atmospheres* 115, D00I16.

5. Friedrich, M., Rapp, M., Blix, T. A., Hoppe, U.-P., Torkar, K. (2011). Electron loss and meteoric dust in the mesosphere. *Proceedings of the 20th ESA Symposium on Rocket and Balloon Programmes and Related Research, Hyères, France, May 2011, Editor Leny Ouwehand, ESA* **SP-700** *(this issue).*

6. Brattli, A., Lie-Svendsen, Ø., Svenes, K., Hoppe, U.-P., Strelnikova, I., Rapp, M., Latteck, R. & Friedrich, M. (2009). The ECOMA 2007 campaign: rocket observations and numerical modeling of aerosol particle charging and plasma depletion in a PMSE/NLC layer. *Ann. Geophys.* 27, 781-796, www.ann-geophys.net/27/781/2009/

7. Brattli, A., Blix, T. A., Lie-Svendsen, Ø., Hoppe, U.-P., Lübken, F.-J., Rapp, M., Singer, W., Latteck, R. & Friedrich, M. (2006). Rocket measurements of positive ions during polar mesosphere winter echo conditions, *Atmos. Chem. Phys.*, 6, 5515–5524, www.atmos-chem-phys.net/6/5515/2006/

8. Bekkeng, T. A. (2009). *Prototype Development of a Multi-Needle Langmuir Probe System.* Master Thesis, University of Oslo, Department of Physics.

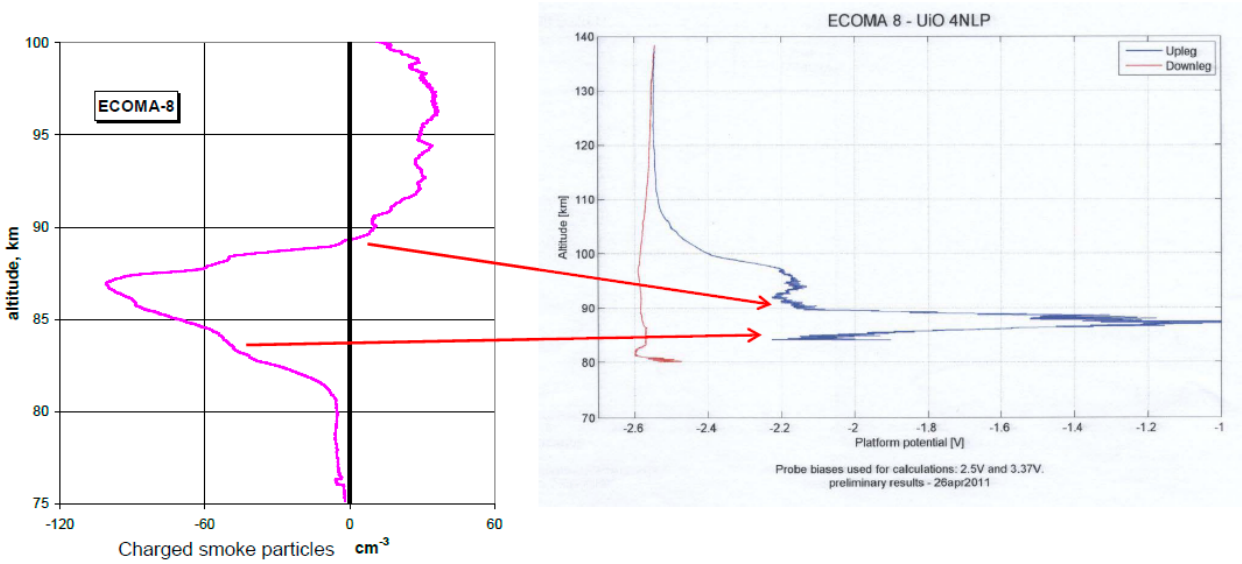

Figure 9. The payload potential becomes less negative in exactly the height region where we observe negatively charged (meteoric) smoke particles with the ECOMA instrument. The red arrows mark the same altitudes in the two panels, which have different altitude scales.

B List of Upcomming Papers

Proposed list of papers for a Special Issue in Annales Geophysicae entitled

"Polar mesospheric structure and composition during the ECOMA 2010 Geminids sounding rocket campaign"

Planned submission deadline: March 30th, 2012

Proposed guest editors: M. Rapp & U.-P. Hoppe

08.11.2011 M. Rapp

---

1. **Meteor observations during the Geminids 2010** Stober et al.

2. **Development of the Na-layer during the Geminids 2010**

   Dunker/Hoppe/Stober/Matthias/Rapp/Plane et al.

3. **Mesospheric NO-observations during ECOMA07** Hedin/Rapp et al.

4. **Turbulence measurements in a mesospheric inversion layer (MIL) and associated wind structures** Szewczyk/Baumgarten/Dunker et al.

5. **Photoelectron spectra and constraints on the properties of MSP**

   Rapp/Hedin/Plane et al.

6. **A multi-instrument comparison of D-region plasma measurements**

   Friedrich/Hoppe/Bekkeng/Rapp et al.

7. **Payload charging effects in the polar D-region associated with MSPs**

   Bekkeng/Hoppe/Friedrich/Barjatya et al.

8. **Electron loss and meteoric dust in the winter polar mesosphere; impact of MSP on the D-region charge balance** Friedrich/Hoppe/Rapp/Hedin/Gumbel et al.

9. **Small scale structures in neutrals and plasma species**

   Strelnikov/Bekkeng/Hoppe/Friedrich et al.

10. **In-situ observations of a highly variable sporadic E-layer** Friedrich/Rapp et al.

C References

APTI (2011). http://www.shodor.org/os411/courses/411b/module02/unit01/page04.html.

Avaste, O. (1993). 'Noctilucent Clouds'. In: *Journal of Atmospheric and Terrestrial Physics* 55(2), pp. 133–143. ISSN: 0021-9169.

Bekkeng, T.A. (2009). 'Prototype Development of a Multi-Needle Langmuir Probe System'. MA thesis. University of Oslo, Department of Physics.

Blix, T.A. (1988). 'In situ studies of turbulence in the middle atmosphere by means of electrostatic ion probes'. PhD thesis. Kjeller, Norway: Norwegian Defence REsearch Establishment, FFI.

Blix., T.A. (2011). Personal communication.

Blix, T.A. and U.-P. Hoppe (2003). 'Existence and charged state of meteoric dust grains in the middle atmosphere (ECOMA)'. Project proposal for the ECOMA campaign.

Chung, P.M., L. Talbot, and J. Touryan (1975). *Electric Probes in Stationary and Flowing Plasmas*. Springer-Verlag New York Inc.

Dubietis, A., P. Dalin, R. Balciunas, K. Cernis, N. Pertsev, V. Sukhodoev, V. Perminov, M. Zalcik, A. Zadorozhny, M. Connors, I. Schofield, T. McEwan, I. McEachran, S. Frandsen, O. Hansen, H. Andersen, J. Gronne, D. Melnikov, A. Manevich, and V. Romejko (2011). 'Noctilucent clouds: modern ground-based photographic observations by a digital camera network'. In: *APPLIED OPTICS* 50(28), F72–F79. ISSN: 0003-6935.

Dunker, T. (2011). 'Effects of meteors and dynamics on the mesospheric sodium layer over Andøya measured with the ALOMAR Na lidar'. MA thesis. University of Oslo and Georg-August-Universität Göttingen.

FRP (2010). *Flight Requirements Plan*. ECOMA campaign 2010, ECOMA No 7/8/9. Andøya Rocket Range.

Folkestad, K. (1970). *Ionospheric studies by in situ measurements in sounding rockets,* tech. rep. NDRE Report no 59. Norwegian Defence Research Establishment,FFI.

Friedrich, M. and M. Rapp (2009). 'News from the Lower Ionosphere: A Review of Recent Developments'. In: *Surveys in Geophysics* 30(6), 525–559. ISSN: 0169-3298. DOI: {10.1007/s10712-009-9074-2}.

Friedrich, M., M. Rapp, J.M.C. Plane, and K.M. Torkar (2010). 'Bite-outs and other depletions of mesospheric electrons'. In: *Journal of Atmospheric and Solar-Terrestrial Physics* 73(14-15, SI), 2201–2211. ISSN: 1364-6826. DOI: 10.1016/j.jastp.2010.10.018.

Friedrich, M., M. Rapp, T.A. Blix, U.-P. Hoppe, and K. Torkar (2011). 'Electron loss and meteoric dust in the mesosphere'. In: presentation at 20th ESA Symposium on European Rocket and Balloon Programmes and Related Research. Hyères, France.

Fritts, D.C. and M.J. Alexander (2003). 'Gravity wave dynamics and effects in the middle atmosphere'. In: *Reviews of Geophysics* 41(1). ISSN: 8755-1209. DOI: {10.1029/2001RG000106}.

Goldberg, RA, DC Fritts, BP Williams, FJ Lubken, M Rapp, W Singer, R Latteck, P Hoffmann, A Mullemann, G Baumgarten, FJ Schmidlin, CY She, and DA Krueger (2004). 'The MaCWAVE/MIDAS rocket and ground-based measurements of polar summer dynamics: Overview and mean state structure'. In: *GEOPHYSICAL RESEARCH LETTERS* 31(24). ISSN: 0094-8276. DOI: {10.1029/2004GL019411}.

Havnes, O., J. Troim, T. Blix, W. Mortensen, L.I. Naesheim, E. Thrane, and T. Tonnesen (1996). 'First detection of charged dust particles in the Earth's mesosphere'. In: *JOURNAL OF GEOPHYSICAL RESEARCH-SPACE PHYSICS* 101(A5), 10839–10847. ISSN: 0148-0227. DOI: {10.1029/96JA00003}.

Hedin, J., J. Gumbel, and M. Rapp (2007). 'On the efficiency of rocket-borne particle detection in the mesosphere'. In: *Atmospheric Chemistry and Physics* 7(14), pp. 3701–3711. DOI: 10.5194/acp-7-3701-2007. URL: http://www.atmos-chem-phys.net/7/3701/2007/.

Hoppe, U.-P., M. Friedrich, T.A. Blix, J.I. Moen, T.A. Bekkeng, K.R. Svenes, . Svendsen, M. Rapp, and K. Torkar (2011a). Personal communication.

Hoppe, U.-P., T.A. Blix, M. Rapp, M. Friedrich, and K. Torkar (2011b). 'The charge balance in the presence of meteoric smoke in the upper mesosphere under summer and winter conditions'. In: presentation at 20th ESA Symposium on European Rocket and Balloon Programmes and Related Research. Hyères, France.

Hoppe, U.-P., M. Friedrich, T.A. Blix, J.I Moen, T.A. Bekkeng, K.R. Svenes, Å. Svendsen, M. Rapp, and K. Torkar (2011c). 'The charge balance in the presence of meteoric smoke in the upper mesosphere under winter conditions-preliminary results'. In: *20th ESA Symposium on European Rocket and Balloon Programmes and Related Research*. Hyères, France, pp. 413–417.

Hunten, D. M., R. P. Turco, and O. B. Toon (1980). 'Smoke and dust particles of meteoric origin in the mesosphere and stratosphere'. In: *Journal of Atmospheric Sciences* 37, pp. 1342–1357. DOI: 10.1175/1520-0469(1980)037<1342:SADPOM>2.0.CO;2.

Kivelson, M.G. and C.T. Russel (1995). 'INtroduction to Space Physics'. In: Cambridge University Press. Chap. 7. Ionospheres.

Lübken, F.J. and U. von Zahn (2001). 'Thermal structure of the mesopause region at polar latitudes'. In: *Journal of Geophysical Research* 96, pp. 841–857.

Murray, B.J. and J. M. C. Plane (2005). 'Uptake of Fe, Na and K atoms on low-temperature ice: implications for metal atom scavenging in the vicinity of polar mesospheric clouds'. In: *Pys. Chem. Chem. Phys.* 7 (23), pp. 3970–3979. DOI: 10.1039/B508846A. URL: http://dx.doi.org/10.1039/B508846A.

Online, Meteor Showers (2011). *Geminids*. http://meteorshowersonline.com/geminids.html.

Physorg (2011). *Geminid meteor shower 2011*. http://www.physorg.com/news/2011-12-geminid-meteor-shower.html.

Rapp, M. (2011). Personal communication.

Rapp, M. and F.J. Lubken (2004). 'Polar mesosphere summer echoes (PMSE): review of observations and current understanding'. In: *ATMOSPHERIC CHEMISTRY AND PHYSICS* 4, 2601–2633. ISSN: 1680-7324.

Rapp, M, FJ Lubken, P Hoffmann, R Latteck, G Baumgarten, and TA Blix (2003). 'PMSE dependence on aerosol charge number density and aerosol size'. In: *JOURNAL OF GEOPHYSICAL RESEARCH-ATMOSPHERES* 108(D8). ISSN: 0747-7309. DOI: {10.1029/2002JD002650}.

Rapp, M., I. Strelnikova, B. Strelnikov, R. Latteck, G. Baumgarten, Q. Li, L. Megner, J. Gumbel, M. Friedrich, U.-P. Hoppe, and S. Robertson (2009). 'First in situ measurement of the vertical distribution of ice volume in a mesospheric ice cloud during the ECOMA/MASS rocket-campaign'. In: *ANNALES GEOPHYSICAE* 27(2), 755–766. ISSN: 0992-7689.

SPL (2011). *Science Photo Library*. http://www.telegraph.co.uk/earth/earthpicturegalleries/5400324/Extraordinary-Clouds-and-The-Cloud-Collectors-Handbook.html?image=6.

Szuszczewicz, Edward P. (1972). 'Area Influences and Floating Potentials in Langmuir Probe Measurements'. In: *Journal of Applied Physics* 43(3), pp. 874 –880. ISSN: 0021-8979. DOI: 10.1063/1.1661297.

von Zahn, U., J. Höffner, V. Eska, and M. Alpers (1996). 'The mesopause altitude: Only two distinct levels worldwide?' In: *Geophysical Research Letters* 23(22), pp. 3231–3234.


UNIVERSITY
OF TROMSØ